BGC ENGINEERING INC.
AN APPLIED EARTH SCIENCES COMPANY

GEOHAZARDS INTERNATIONAL

CO-SEISMIC LANDSLIDE SUSCEPTIBILITY MAP FOR THE KINDGOM OF BHUTAN

FINAL

PROJECT NO.: BGC21006 DATE: May 27, 2022

BGC ENGINEERING INC.
AN APPLIED EARTH SCIENCES COMPANY
Suite 500 - 980 Howe Street
Vancouver, BC Canada V6Z 0C8
Telephone (604) 684-5900
Fax (604) 684-5909

May 27, 2022
Project No.: BGC21006

Heidi Stenner
GeoHazards International
687 Bay Road, Menlo Park,
California 94025 USA

Dear Heidi,

Re: Co-seismic landslide susceptibility map for the Kingdom of Bhutan

Attached is BGC Engineering Inc.'s report in support of co-seismic landslide susceptibility mapping in Bhutan. We appreciate the opportunity to work with GeoHazards International on such a challenging and interesting project.

Yours sincerely,

BGC ENGINEERING INC.
per:

Kris Holm, M.Sc., P.Geo.
Principal Geoscientist

EXECUTIVE SUMMARY

BGC Engineering Inc. (BGC), in partnership with GeoHazards International (GHI)**,** has developed a regional coseismic landslide susceptibility model and map for the Kingdom of Bhutan (Bhutan), which considers seismic shaking data for two different earthquake scenarios generated for GHI by Verisk Analytics.

A regional coseismic landslide susceptibility model estimates landslide likelihood given the occurrence of specific degrees of shaking from an earthquake. Maps are an output of the model, and display expected spatial landslide distribution associated with an earthquake. The intended use of such a model and map for Bhutan is to inform work by authorities and practitioners related to country-scale land use planning, development regulation, and emergency management in terrain prone to seismic-triggered landslides. Specifically, the work is intended to inform where landslides may be more or less likely to occur during the earthquake scenarios considered in this study – information that can support regional to country-scale risk management decision making.

The purpose of coseismic landslide susceptibility modelling is to illustrate landslide likelihood given the occurrence of specific degrees of shaking from an earthquake. To produce this output, a data-driven model was developed that ingests geospatial data representing coseismic landslides, the seismic data associated with their respective earthquake events, and a range of topographic, geologic, and thematic data. These data are used within the model to find relationships between ground shaking, terrain conditions, and earthquake-triggered landslide occurrence, and the map is an output of the model.

Two earthquake scenarios provided by Verisk Analytics were tested for this study. According to information provided by GHI, one scenario is a magnitude 7 (M7) earthquake occurring along the Dhubri-Chungthang right-lateral strike slip fault in Southwestern Bhutan. This scenario was reportedly modeled after a 1980 M6.3 earthquake that occurred at a depth of 45 km. The M7 scenario earthquake is interpreted to occur along the same fault zone but at a shallower depth, occurring at 12 km and rupturing to the surface, as this could be a potentially more damaging example of an earthquake for southwestern Bhutan.

The second scenario is a M8 earthquake that represents a hypothetical repeat of the 1714 ~M8 earthquake along the Main Himalayan Thrust fault along the southern border of Bhutan. This scenario is estimated to occur at a depth of 10 km and with a northerly dip of 10 degrees, rupturing the fault from the surface to a depth of 20 km.

For the Kingdom of Bhutan, we considered a recorded M6.1 earthquake in eastern Bhutan from 2009 plus the two hypothetical scenario earthquakes and found:

- For an equivalent of the M6.1 event in 2009, we expect about 18 landslides to have occurred nation-wide, including 5 along roads and 1 along national highways.
- For an equivalent of the M7 scenario, we expect about 750 to 3,650 landslides nation-wide, concentrated near the source fault along the west border of Bhutan. Of these, about 20 to 60 landslides are expected to occur within 200 m of national highways.

- For an equivalent of the M8 scenario, we expect about 36,000 to 41,000 landslides nation-wide, concentrated in the southern half of Bhutan. Of these, 600 to 1,200 landslides are expected to occur within 200 m of national highways.

The models have a number of specific limitations, including:

- They have been developed with a nominal resolution of 30 m. Very limited meaning, if any, can be taken from the map for any area smaller than about 500 m by 500 m.
- The results of this study can help understand where landslides may occur following a specific earthquake with known location and magnitude, but they give no insight as to where or when a landslide-triggering earthquake may occur.
- The coseismic landslide susceptibility models presented in this report give a forecast of expected landslide distribution, in space, associated with a specific earthquake event. Each model is specific to a given earthquake scenario and does not apply to any other earthquake.
- The models are unable to distinguish between different landslide types.

Although subject to limitations, the results of this study show that existing United States Geological Survey (USGS) global models for coseismic landslide susceptibility can be improved through the use of higher resolution topographic data, the inclusion of additional explanatory variables, and the use of a range of analytical models.

The models produced in this work are intended to be used at a national scale in Bhutan, with the following intended uses:

- Education and awareness
- Disaster response planning
- Prioritization of more detailed region-specific or site-specific study.

BGC makes the following recommendations for potential future work to improve the model results:

1. Include more events in the model training.
2. Allow for different weighting of events.
3. Proximity to road cuts.
4. Include features that account for position relative to the fault.
5. Include information about antecedent soil moisture conditions.
6. Include PGV and MMI in results for Bhutan scenario earthquakes.
7. Include higher resolution regional data.
8. Compile coseismic landslide data for the Kingdom of Bhutan.

BGC makes the following recommendations for future work to improve the use of results in decision making:

1. Compare results to building locations, settlements or infrastructure to prioritize further assessment.
2. Develop a plan to incorporate results into planning, policy, and emergency management**.**

TABLE OF CONTENTS

LIST OF TABLES

LIST OF FIGURES

LIST OF APPENDICES

LIST OF DRAWINGS

1.0 INTRODUCTION

BGC Engineering Inc. (BGC), in partnership with GeoHazards International (GHI), has developed a regional coseismic landslide susceptibility model and map (the map) for the Kingdom of Bhutan (Bhutan), which considers seismic shaking data for two different earthquake scenarios generated for GHI by Verisk Analytics.

A regional coseismic landslide susceptibility model estimates landslide likelihood given the occurrence of specific degrees of shaking from an earthquake. Maps are an output of the model, and display expected spatial landslide distribution associated with an earthquake. The intended use of such a model and map for Bhutan is to inform work by authorities and practitioners related to country-scale land use planning, development regulation, and emergency management in terrain prone to seismic-triggered landslides. Specifically, the work is intended to inform where landslides may be more or less likely to occur during the earthquake scenarios considered in this study – information that can support regional to country-scale risk management decision making.

The main document of this report summarizes the study objectives, methods, results, and limitations at a level of detail intended for authorities and practitioners. Appendix A provides a more detailed and quantitative description of the work for subject matter experts.

BGC notes that the results of this study could be presented in different formats depending on the use-case. BGC intends to present this work to GHI, subject matter experts and authorities within Bhutan to develop an understanding of the intended use-cases and, if necessary, reformat the results to suit the needs of the end-users.

1.1. Study Area

The Kingdom of Bhutan is in a mountainous and seismically active region. It is a landlocked nation in the Eastern Himalayas, sharing borders with India to the south and east and Tibet to the north. The Bhutanese people live with a heightened sense of awareness of the seismically induced hazards following the 2015 Gorkha Earthquake in Nepal. This devastating earthquake had a moment magnitude of 7.8 and was caused by a thrust along the Main Himalayan Fault, which is the fault carrying the Indian Plate under the Eurasian Plate along both the Nepalese and Bhutanese southern borders. Due to its location in an active seismic zone, steep sloping terrain, and variable climatic conditions, Bhutan is prone to a wide spectrum of natural hazards including landslides, snow avalanches, floods, and seismic events.

1.2. Scope of Work

The scope of work was outlined in a proposal submitted to GHI by BGC on February 23, 2021**.** The technical aspects of the work were broadly divided into three tasks, which are described briefly as follows:

- Task 1: Data compilation and data review.
    - Characterization of the study area by reviewing existing reports, geology, terrain, landslide, climate, seismic, and hydrologic information, and compiling remotely-sensed (e.g., LiDAR and air photos) and basemap data in GIS format.

  - Compilation of data and baseline analyses required for assessment. This includes topographic, terrain, hydrologic, seismic, geomorphologic analyses, and consideration of climate change impacts.

- Task 2: Model Development.
  - Completion of landslide susceptibility mapping using a range of conventional statistical methods and machine learning approaches.
  - Generation of Model Outputs.
  - Validation of Model Results.
- Task 3: Reporting.
  - Dissemination of co-seismic landslide susceptibility maps and data in digital (PDF) and web-accessible format (Cambio Communities) amenable to incorporation into policy and risk-informed decision making.
  - Presentation of results to Bhutan authorities, subject matter experts and GHI.

2.0 METHODOLOGY

2.1. Modelling Approach

The purpose of coseismic landslide susceptibility modelling is to illustrate landslide likelihood given the occurrence of specific degrees of shaking from an earthquake. To produce this output, a data-driven model was developed that ingests geospatial data representing coseismic landslides, the seismic data associated with their respective earthquake events (i.e., USGS shakemap), and a range of topographic, geologic, and thematic data. These data are used within the model to find relationships between ground shaking, terrain conditions, and earthquake-triggered landslide occurrence, and the map is an output of the model.

Reichenbach et al. (2018) provide a start of the art review of statistical methods for landslide susceptibility mapping, including a thorough discussion of the selection of explanatory variables to be considered for use in the model. With that framework in mind, we consulted a range of recent literature focusing on coseismic landslide susceptibility maps and completed a survey of variables used in recent models. Our findings are summarized in Table 2-1, which was generated from a review of 11 recent coseismic landslide susceptibility studies.

There are many published studies that examine the relationship between parameters such as those listed in Table 2-1 and coseismic landslides at the regional scale (e.g., encompassing all or part of a country). However, the model developed for this study is at a global-scale. Spatial datasets containing inventories of coseismic landslides are relatively scarce, especially when considering a single region. Therefore, the benefit to the global-scale model approach is that one can leverage all available data, rather than only data for a specific region. This benefit needs to be balanced with careful consideration of the potential for variability in local conditions that are indicative of coseismic landsliding. Nowicki Jesse et al (2018) developed a global-scale coseismic landslide susceptibility model that uses a linear regression technique. The Nowicki Jesse et al. (2018) model was approximately replicated for this study, in addition to development of a tree-based machine learning model and a weights of evidence model, as discussed in greater detail in Appendix A.

Development of a landslide susceptibility map can be completed by a range of methods, including deterministic (i.e., slope stability analysis), heuristic (i.e., spatial factors weighted and combined according to judgement), inventory-based (i.e., considering solely the spatial distribution of mapped landslides) and statistical (i.e., comparison of mapped landslides with other spatial data to develop relationships and combine them to produce a map). These methods generally produce a map with a unitless numerical scale ranging between arbitrary lower and upper values representing the likelihood of ground movement given an earthquake event. These values can be reclassified into a smaller number of classes with specific statistical meaning and translated to qualitative expressions of hazard likelihood (e.g., high, medium, low). Where sufficient data are available, they may also be transformed to give an estimate of the spatial frequency of landslide presence across the map.

Table 2-2 provides an overview of the datasets considered within the model developed for this study. There are no coseismic landslide inventories available for Bhutan, and so the model could not be validated directly for Bhutan. As the best approximate proxy, the magnitude 7.8 earthquake that occurred in Nepal on April 25, 2015 was selected (the 'Gorkha' event). This event was left out of all model training, validation, and testing steps. The accuracy of the model as applied to this case is thought to be the best approximation for how the same model could perform for an earthquake occurring in Bhutan given the model had not included any Bhutanese or Nepalese data during training. The purpose of this approach is to first build confidence in the model within the Himalayan Region before applying the model to earthquake scenarios for the Kingdom of Bhutan and producing coseismic landslide susceptibility maps for use by Bhutanese Authorities, GHI or other parties.

Table 2-1. Summary of parameters used in recent coseismic landslide susceptibility studies.

	Amato et al 2021	Casagli et al 2021	Cauzzi et al 2018	Chen et al 2021	Nowicki Jessee et al 2018	Lambardo and Tanyas 2020	Massey et al 2020	Pokharel et al 2020	Polykreti et al 2019	Shao et al 2019	Tanyas et al 2019a	Tanyas et al 2019b	This Study
PGA			✓	✓	✓	✓		✓	✓	✓	✓	✓	✓
Fault distance	✓						✓		✓	✓			
Peak Ground Velocity (PGV)					✓		✓	✓			✓		✓
Epicentral distance										✓			
Magnitude					✓						✓		
Modified Mercalli Index					✓			✓			✓		✓
Elevation	✓		✓		✓		✓		✓	✓			✓
Slope angle	✓		✓	✓	✓	✓	✓	✓	✓	✓	✓	✓	✓
Aspect	✓		✓	✓					✓	✓			✓
Local relief	✓					✓	✓	✓			✓	✓	✓
Profile curvature	✓					✓		✓		✓	✓		✓
Plan curvature	✓					✓		✓		✓			✓
Roughness	✓					✓		✓			✓		
Precipitation		✓											✓
Wetness	✓				✓			✓			✓		✓
Distance to Watercourse				✓		✓				✓	✓		
Lithology	✓			✓	✓		✓		✓	✓		✓	✓
Landcover				✓	✓				✓				✓
Distance to Roads	✓								✓	✓			
Geomorphon class	✓							✓					
Soil Type	✓			✓									

Figure 2-1 provides a high-level overview of the study workflow. An overview of the coseismic landslide databases used within the model and a detailed summary of the model workflow and validation are provided in Appendix A. Once the relationships between physiographic setting and landslide occurrence were quantified using this model, they were then applied to the regional scale to produce estimated susceptibility as a function of the local Bhutanese physiographic setting. Section 4.0 discusses implications of the resolution of input parameters used for this study.

Table 2-2. Summary of parameters used for this study.

Category	Variable	Data Type	Source	Spatial Resolution
Seismic Derivatives	Peak Ground Acceleration (PGA)	Continuous raster	USGS ShakeMap System (Worden & Wald, 2016)	1 km
	Peak Ground Velocity (PGV)			
	Modified Mercalli Intensity (MMI)			
Topographic Derivatives	Elevation	Continuous raster	Shuttle Radar Topography Mission	30 m
	Slope Angle			
	Relative Slope Aspect[1]			
	Local Relief			
	Curvature (plan, profile, combined)			
	Compound Topographic Index			
Precipitation	Average Annual Precipitation	Continuous raster	WorldClim Mean Monthly Precipitation	30 arc-seconds
Aridity	Annual average reference evapotranspiration	Continuous raster	Trabucco and Zomer (2018)	30 arc-seconds
	Annual average aridity index			
Vegetative cover	Percentage green vegetation cover	Continuous Raster	Broxton, Zeng, Scheftic, and Troch (2014)	30 arc-seconds
Lithology	GLiM Global Lithology Data	15-class categorical vector	Hartmann and Moosdorf (2012)	Extracted from a vector dataset (approximately 1:1,000,000 scale)
Landcover	Globecover 2009 Landcover	20-class categorical raster	Arino et al. (2012)	300 m

Notes:
1. Relative Aspect is a measure of the slope aspect for a given point relative to the location of the earthquake epicentre
2. Compound Topographic Index is a measure of topographic wetness calculated by applying hydrologic principles to the interpretation of topographic data

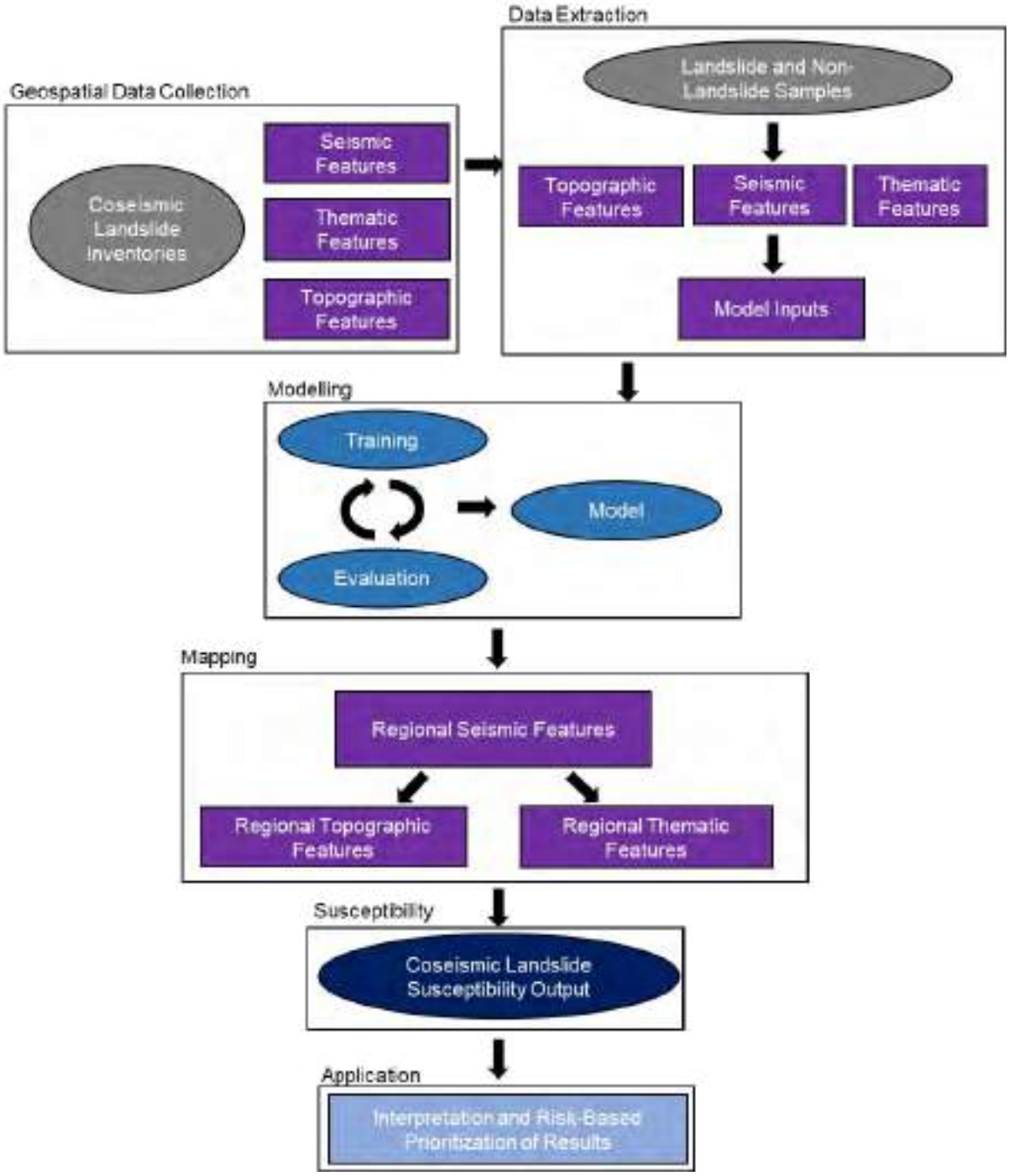

Figure 2-1. Overview of methodology for creating a regional coseismic landslide susceptibility map for Bhutan.

2.2. Earthquake Scenarios

Two earthquake scenarios provided by Verisk Analytics were tested for this study. According to information provided by GHI, one scenario earthquake is a M7 occurring along the Dhubri-Chungthang right-lateral strike slip fault in Southwestern Bhutan. This scenario was modeled after

a 1980 M6.3 earthquake that occurred at a depth of 45 km. The M7 scenario earthquake is interpreted to occur along the same fault zone but at a shallower depth, occurring at 12 km and rupturing to the surface, as this could be a potentially more damaging example of an earthquake for southwestern Bhutan.

The second scenario earthquake is a M8 that represents a hypothetical repeat of the 1714 ~M8 earthquake along the Main Himalayan Thrust fault along the southern border of Bhutan. This scenario is estimated to occur at a depth of 10 km and with a northerly dip of 10 degrees, rupturing the fault from the surface to a depth of 20 km.

3.0 RESULTS

Drawing 001 and Drawing 002 (attached) present the results as a country-scale co-seismic landslide hazard susceptibility map for two earthquake scanrios. For greater ease of navigation, BGC also presents the map on a web application, Cambio, which can be accessed at **www.cambiocommunities.ca**. New users will need to click “register for access” to obtain login information. BGC has also provided map data in a separate file as an ESRI Geodatabase. The map portrays landslide susceptibility as function of number of expected landslides per unit area. Drawing 001 and Drawing 002 are provided at 1:2,000,000 scale. The web version provided on Cambio is intended to be viewed at province to country scale; the results should not be relied upon at the scale of specific assets.

Appendix A provides a detailed account of the modelling methodology, interpretation of the model outputs and their intended use. Key technical findings of the work summarized in Appendix A include:

- Model performance for the Logistic Regression (LR) and Light Gradient Boosted Machine (LGBM) models has been evaluated qualitatively, through visual inspection, and quantitatively through the use of balanced accuracy metrics and area under the receiver operating characteristic curves:
    - Model performance is shown to be generally good, comparable to and better than that of the United States Geological Survey (USGS) models based on coarser topographic data.
    - Optimum decision thresholds vary proportional to earthquake magnitude and associated ground shaking parameters (i.e., PGA, PGV and MMI).
    - Model performance may vary across the range of model earthquake events, and models may need to be adjusted for local considerations to optimize them for use in a specific region.
- With consideration of the 2010 Haiti M7.0 earthquake, which was included as a validation case for the model:
    - Our LGBM, LR and WoE models outperform three results available from USGS, including that based on the work of Nowicki Jessee et al. (2018). An ensemble model that combines the LGBM, LR and Weights of Eveidenc (WoE) models in equal weight also outperforms the USGS models.
    - An estimate of spatial density of landslides from the event produces a lower estimate (average estimate of 3,560 landslides) than the number (i.e., 23,568) documented by Harp et al. (2017).
- With consideration of the 2015 Gorkha (Nepal) M7.8 earthquake, which was not included in training/developing the model but was used to test the model's ability to accurately predict the landslides that occurred during the earthquake**.**
    - All BGC models (i.e., LGBM, LR, WoE and an ensemble model) outperform the USGS models by a wide margin.
    - An estimate of spatial density of landslides from the event by our model produces similar estimates (range from 29,032 to 62,359 landslides) to those (i.e., 24,795)

documented by Roback et al. (2017). This good agreement gives us high confidence in the model's predictive power for nearby Bhutan with similar terrain.

3.1. Key Findings: Model Output for Bhutan Earthquake Scenarios

For the Kingdom of Bhutan, we considered a M6.1 earthquake in eastern Bhutan from 2009 plus two scenario earthquakes with available PGA shakemaps and found:

- For the M6.1 event our most confident prediction, based on the WoE model, is for 18 landslides[1] nation-wide, 5 along roads which includes 1 along national highways.
- For the M7 scenario, we expect from 754 to 3,649 landslides nation-wide, concentrated near the source fault along the west border of Bhutan. Of these, 20 to 56 landslides are expected to occur within 200 m of national highways.
- For the M8 scenario, we expect from 35,873 to 40,885 landslides nation-wide, concentrated in the southern half of Bhutan. Of these, 604 to 1,150 landslides are expected to occur within 200 m of national highways.

These results are summarized in Table 3-1 below, where we summarize estimates for landslides in Bhutan associated with the three different earthquake scenarios under consideration, for each considered model. We distinguish between the total numbers of landslides expected across the whole Kingdom of Bhutan and those to be found within 200 m (i.e., 400 m wide corridor) along roads or national highways.

Landslide predictions for the whole of Bhutan for the M8 scenario earthquake range between 35,873 and 40,885. We may therefore expect that a M8 earthquake occurring along the southern border would likely produce widespread landslides, being potentially more widespread than those in Nepal following the 2015 Gorkha event. By contrast, the M7 scenario is expected to produce an order of magnitude fewer landslides, with an ensemble model forecast of 2,196 landslides, of which 38 are expected along national highway corridors.

[1] At the resolution of study, the model is not able to differentiate between landslide types. Landslide point locations identified at the scale of the model do not represent landslide extent or failure characteristics (e.g., multiple points of rockfall detachment, or slope failure within a larger landslide complex).

Table 3-1. Expected landslides for Bhutan earthquake scenario events.

Event	Model	Estimated Number of Landslides		
		Whole Bhutan	All roads (within 200 m)	National Highways (within 200 m)
2009 M6.1	Ensemble	263	26	6
	WoE	18	5	1
	LGBM	222	29	6
	LR	548	44	11
M7 Scenario	Ensemble (PGA only)	2196	144	38
	LR (PGA only)	3649	200	56
	WoE (PGA only)	754	88	20
M8 Scenario	Ensemble (PGA only)	38334	3998	877
	LR (PGA only)	35873	2716	604
	WoE (PGA only)	40885	5292	1150

4.0 INTENDED USE OF THE MODEL OUTPUT

4.1. Interpretation of the Model Results

The results of this modelling work show that existing USGS global models for coseismic landslide susceptibility can be improved through the use of higher resolution topographic data, the inclusion of additional explanatory variables, and the use of a range of analytical models. We consider that this work has been successful in its initial objective to build on the work of Nowicki Jessee et al. (2018) to obtain a global model with higher predictive power.

Any global model has certain advantages and disadvantages. An advantage is that it can be applied anywhere in the world in the event of a potentially landslide-producing earthquake, without the need to build a new custom model for a specific area under time pressure following an event. A potential disadvantage of a global model is that it is based on observed landslides and terrain conditions from across the globe, and therefore represents an average model, that may be relatively good everywhere, but with potentially high variability in predictive power for specific locations. A global model's results may be very poor in areas where the average terrain characteristics are significantly different than the average characteristics for events included in the model. In the present work, we see that our models are somewhat better than USGS models for a 2010 Haiti earthquake, and much better for the 2015 Gorhka, Nepal earthquake, based on the statistical evaluation provided in Appendix A. We also see that our predictions for expected number of landslides are relatively poorly aligned for the Haiti event and very good for the Nepal event, relative to available inventories of mapped landslides. Further detailed examination of model performance across the range of events included in our models is expected to show variable model performance. **Given the models' good performance for Nepal, we expect similar good performance for nearby Bhutan, based on its similar geology and physiography, at least for the mountainous areas of northern Bhutan.**

The models produced in this work are intended to be used at a national scale in Bhutan, with the following intended uses:

- Education and awareness
- Disaster response planning
- Prioritization of more detailed region-specific or site-specific study.

4.2. Model Limitations

The models have been developed with a nominal resolution of 30 m. This resolution is based on that of the topographic data set, which is the highest resolution data included in the model. The practical resolution of the model may be as poor as the lowest resolution dataset included in the model, which is a 1 km grid for the seismic load parameters included in the USGS shakemaps. Among the terrain variables, which are static, remaining unchanged with changes in earthquake load, several inputs (i.e., precipitation, aridity and vegetative cover) have a resolution of 30 arc seconds, which can be as long as ~ 900 m near the equator. The global land cover model has a resolution of 300 m. The practical resolution of the model is therefore between 30 m and 1 km,

with 500 m perhaps representing a reasonable best estimate. We consider that the model is useful at a global or national scale for identifying wide trends but should not be used at larger (more detailed) scale. **Very limited meaning, if any, can be taken from the map for any area smaller than about 500 m by 500 m**. Region-specific maps may have potential for improvement with the benefit of larger scale (higher resolution) input data for lithology, land cover, soil moisture or other terrain characteristics.

A landslide susceptibility map developed using statistical methods with the benefit of an existing landslide inventory gives an estimate of the expected spatial distribution of landslides across the map. It gives no information on temporal probability, or the expected frequency of landslides in time; rather it only tells where, in space, landslides are more or less likely. The results of this study therefore help understand **where** landslides may occur following a specific earthquake with known location and magnitude, but they give no insight as to **where or when** a landslide-triggering earthquake may occur.

The coseismic landslide susceptibility models presented in this report give a **forecast of expected landslide distribution, in space, associated with a specific earthquake event**. The model is specific to a given earthquake scenario and does not apply to any other earthquake. That said, a significant proportion of the model – that associated with unchanging terrain conditions - remains constant across models for all earthquake events; only the seismic load component of the model is event-specific. The model can be re-run for any other scenario earthquake event with an available Shakemap, including any future earthquake affecting Bhutan for which USGS publishes a Shakemap. For this exercise, the model was tested using two earthquake scenarios that were provided by a third party, however, other earthquake scenarios are possible within Bhutan.

The models are unable to distinguish between different landslide types. The model training data are generally unspecific about landslide type, and where sub-classification data are available, they are classified inconsistently across datasets. The models therefore only predict relative likelihood of a non-specific landslide type to occur. This may conceal important differences in landslide likelihood across the range of landslide types. This means that the landslides triggered by earthquakes as modelled for this study could include a broad range of gravitational slope failures including, for example, rockfall, rockslide, earth slide and debris slide.

4.3. Potential Model Improvements

This project has produced a coseismic landslide susceptibility model that was used to produce coseismic landslide susceptibility maps for specific earthquake scenarios for the Kingdom of Bhutan. BGC makes the following recommendations for future work to improve the model results:

1. **Include more events in the model training:** 25 earthquake events with landslide inventory data were included in this model. Increasing the number of examples that the model is given may improve its performance.
2. **Allow for different weighting of events:** Events were taken from all around the world, and when running the model for a specific area for Bhutan, one might expect

improvements if events and areas more like Bhutan are weighted more heavily during the model training.

3. **Proximity to road cuts:** One feature that may help to explain the presence of coseismic landslides would be proximity to road cuts or other similar features where anthropogenic steepening has occurred. This type of information should be included in the model where possible.
4. **Include features that account for position relative to the fault:** Experience in the literature suggests that one could expect more landslides to occur with different likelihood on the hanging wall of the fault as compared with the foot wall. Including this may help reduce false positive rates in the model.
5. **Include information about antecedent soil moisture conditions:** It is likely that soil moisture has played some role in the documented occurrence of coseismic landslides. Presently, it is challenging to compile this information given geographic and temporal extents of the inventories, but the relationship between antecedent precipitation and coseismic landslides could be explored for more the recent inventories with the benefit of satellite-based soil moisture models. Future development of this model could explore the inclusion of moisture conditions leading up to a particular earthquake event.
6. **Include PGV and MMI in results for Bhutan scenario earthquakes:** Both PGA and PGV were shown to be important predictors for the LR and LGBM coseismic landslide model, and MMI was also important in the WoE model. Performance for models with only PGA was worse in the global validation. Currently, only PGA is computed for the M7 and M8 earthquake scenarios in Bhutan. It is recommended that both PGA and PGV be produced for those earthquake scenarios in Bhutan to provide a better basis for scenario-based landslide models.
7. **Include higher resolution regional data.** It may be possible to improve on the model for Bhutan by including larger scale data for factors like lithology and land cover in place of global data sets. Such a substitution would require some degree of judgement in place of statistical analysis, since those data could not be compared to the other globally available event data. This would introduce some uncertainty in the model, but possibly with the benefit of improved predictive power.
8. **Compile coseismic landslide data for the Kingdom of Bhutan.** As noted, the model was not calibrated within Bhutan because of a lack of available data, however, if such data does exist it could be used to further calibrate the model for use in Bhutan.

5.0 RECOMMENDATIONS

BGC makes the following recommendations for future work to improve the use of results in decision making:

1. **Compare results to building locations, settlements or infrastructure to prioritize further assessment.** Hazard exposure assessment could help focus further analyses to improve the model results in higher priority areas, such as individual buildings, settlements or hillsides. Moreover, these results can be used to help Bhutanese authorities to decide where more detailed site assessment is required prior to development or other investment in a given location.
2. **Develop a plan to incorporate results into planning, policy, and emergency management.** BGC suggests that the results of this work be considered alongside other geohazards present within Bhutan (e.g., floods, precipitation-triggered landslides, and wildfires) in a framework for geohazard risk management. Such work might also include the preparation of hazard maps in formats intended for use in land use regulation. The results of this study can be used at a high level for planning where settlements and other development investments would minimize exposure to co-seismic landslide hazards, and such decisions could be incorporated into land use policy, for example.

6.0 CLOSURE

BGC Engineering Inc. (BGC) prepared this document for the account of GeoHazards International. The material in it reflects the judgment of BGC staff in light of the information available to BGC at the time of document preparation. Any use which a third party makes of this document or any reliance on decisions to be based on it is the responsibility of such third parties. BGC accepts no responsibility for damages, if any, suffered by any third party as a result of decisions made or actions based on this document.

As a mutual protection to our client, the public, and ourselves all documents and drawings are submitted for the confidential information of our client for a specific project. Authorization for any use and/or publication of this document or any data, statements, conclusions or abstracts from or regarding our documents and drawings, through any form of print or electronic media, including without limitation, posting or reproduction of same on any website, is reserved pending BGC's written approval. A record copy of this document is on file at BGC. That copy takes precedence over any other copy or reproduction of this document.

Yours sincerely,

BGC ENGINEERING INC.
per:

Richard Carter, M.Sc.
Geohazard Specialist

Pete Quinn, Ph.D., P.Eng.
Principal Geotechnical Engineer

Rudy Schueder, M.A.Sc., EIT
Data Scientist

Reviewed by**:**

Kris Holm, M.Sc., P.Geo.
Principal Geoscientist

Autumn Umanetz, M.ASc., P.Eng.
Data Scientist

RC/AU/mjp/mm

REFERENCES

Alfaro, P., Delgado, J., Garcia-Tortosa, F. J., Lenti, L., Lopez, J. A., Lopez-Casado, C., & Martino, S. (2012). *Widespread landslides induced by the Mw 5.1 earthquake of 11 May 2011 in Lorca, SE Spain* [GIS data]. Retrieved from the U.S. Geological Survey website: **https://www.sciencebase.gov/catalog/item/5b5a11e7e4b0610d7f4dcb7c.**

Arino, O., Ramos P., Jose J., Kalogirou, V., Bontemps, S., Defourny, P, Van Bogaert, E. (2012): Global Land Cover Map for 2009 (GlobCover 2009). © European Space Agency (ESA) & Université catholique de Louvain (UCL), PANGAEA, https://doi.org/10.1594/PANGAEA.787668

Amato, G., Fiorucci, M., Martino, S., Lombardo, L., & Palombi, L. (n.d.). Earthquake-triggered landslide susceptibility in Italy by means of Artificial Neural Network.

Bonham-Carter, G.F., Agterberg, F.P, & Wright, D.F. (1989). Weights of evidence modelling: a new approach to mapping mineral potential. In F.P Agterberg & G.F. Bonham-Carter (Eds.), Statistical applications in the earth sciences (Geological Survey of Canada Paper 89-9, pp. 171-183). Ottawa, Ontario: Geological Survey of Canada.

Broxton, P. D., Zeng, X., Scheftic, W., & Troch, P. A. (2014). A MODIS-based global 1-km maximum green vegetation fraction dataset. *Journal of Applied Meteorology and Climatology*, *53*(8), 1996-2004. https://doi.org/10.1175/JAMC-D-13-0356.1

Casagli, N., Intrieri, E., Carlà, T., di Traglia, F., Frodella, W., Gigli, G., Lombardi, L., Nocentini, M., Raspini, F., & Tofani, V. (2021). Monitoring and Early Warning Systems: Applications and Perspectives (pp. 1–21). **https://doi.org/10.1007/978-3-030-60311-3_1**

Cauzzi, C., Fäh, D., David, •, Wald, J., Clinton, J., Losey, S., & Wiemer, S. (n.d.). ShakeMap-based prediction of earthquake-induced mass movements in Switzerland calibrated on historical observations. Natural Hazards. **https://doi.org/10.1007/s11069-018**

Chen, S., Miao, Z., Wu, L., Zhang, A., Li, Q., & He, Y. (2021). A One-Class-Classifier-Based Negative Data Generation Method for Rapid Earthquake-Induced Landslide Susceptibility Mapping. Frontiers in Earth Science, 9. https://doi.org/10.3389/feart.2021.609896

Gnyawali, K.R., & Adhikari, B.R. (2017*). Earthquake induced landslides triggered by 2015 Gorkha earthquake Mw 7.8* [GIS data]. Retrieved from the U.S. Geological Survey website: **https://doi.org/10.5066/F7028Q2X**.

Gorum, T., Korup, O., van Westen, C. J., van der Meijde, M., Xu, C., & van der Meer, F. D. (2017). *Landslides triggered by the 2002 Denali earthquake, Alaska* [GIS data]. Retrieved from the U.S. Geological Survey website: **https://doi.org/10.5066/F7G73C76**.

Gorum, T., Korup, O., van Westen, C. J., van der Meijde, M., Xu, C., & van der Meer, F. D. (2017). *Landslides triggered by the 2007 M 6.2 Aisen, Chile earthquake* [GIS data]. Retrieved from the U.S. Geological Survey website: **https://doi.org/10.5066/F7125R5V**.

Harp, E.L., Hartzell, S.H., Jibson, R.W., Ramirez-Guzman, L., & Schmitt, R.G. (2017*). Landslides triggered by the October 15, 2006, M 6.7 Kiholo Bay, Hawaii, earthquake* [GIS data]. Retrieved from the U.S. Geological Survey website: **https://doi.org/10.5066/F74Q7SH0**.

Harp, E.L., & Jibson, R.W. (2017*). Inventory of landslides triggered by the 1994 Northridge, California earthquake* [GIS data]. Retrieved from U.S. Geological Survey website: **https://doi.org/10.5066/F7Z60MKF**.

Harp, E.L., Jibson, R.W., & Schmitt, R.G. (2017). *Map of landslides triggered by the January 12, 2010, Haiti earthquake* [GIS data]. Retrieved from the U.S. Geological Survey website: https://doi.org/10.5066/F7C827SR.

Harp, E.L., & Keefer, D.K. (2017). *Landslides triggered by the Coalinga, California, earthquake of May 2, 1983* [GIS data]. Retrieved from the U.S. Geological Survey website: **https://doi.org/10.5066/F7G73C76**.

Harp, E.L., Wilson, R.C., & Wieczorek, G.F. (2017). *Landslides from the February 4, 1976, Guatemala earthquake* [GIS data]. Retrieved from the U.S. Geological Survey website: **https://doi.org/10.5066/F7VD6X0Z**.

Hartmann, **J.,** Moosdorf, N. **(2012):** The new global lithological map database GLiM: A representation of rock properties at the Earth surface. *Geochemistry, Geophysics, Geosystems*, **13**, Q12004, https://doi.org/10.1029/2012GC004370

Keefer, D.K., & Manson, M.W. (2017). *Landslides generated by the Loma Prieta, California, earthquake of October 17, 1989* [GIS data]. Retrieved from the U.S. Geological Survey website: **https://doi.org/10.5066/F76Q1VR9**.

Lombardo, L., & Tanyas, H. (2020). From scenario-based seismic hazard to scenario-based landslide hazard: fast-forwarding to the future via statistical simulations. http://arxiv.org/abs/2004.00537

Martino, S., Prestininzi, A., & Romeo,R.W. (2014). *Earthquake-induced ground failures in Italy from a reviewed database* [GIS data]. Retrieved from the U.S. Geological Survey website: https://www.sciencebase.gov/catalog/item/5b6b26b0e4b006a11f779680.

Martino, S., Prestininzi, A., & Romeo,R.W. (2014) *Earthquake-induced ground failures in Italy from a reviewed database* [GIS data]. Retrieved from the U.S. Geological Survey website: **https://www.sciencebase.gov/catalog/item/5b5f6a4be4b006a11f66ece9**.

Massey, C. I., Townsend, D. T., Lukovic, B., Morgenstern, R., Jones, K., Rosser, B., & de Vilder, S. (2020). Landslides triggered by the MW7.8 14 November 2016 Kaikōura earthquake: an update. Landslides, 17(10), 2401–2408. https://doi.org/10.1007/s10346-020-01439-x

Ministerio de Medio Ambiente y Recursos Naturales, El Salvador. (2017). *Landslide inventory for the February 13, 2001, San Salvador, El Salvador earthquake* [GIS data]. Retrieved from the U.S. Geological Survey website: **https://doi.org/10.5066/F7K072SP**.

Morton, D.M. (2017). *Seismically triggered landslides in the area above the San Fernando Valley* [GIS data]. Retrieved from the U.S. Geological Survey website: https://doi.org/10.5066/F7057DFS.

Nowicki Jessee, M. A., Hamburger, M. W., Allstadt, K., Wald, D. J., Robeson, S. M., Tanyas, H., Hearne, M., & Thompson, E. M. (2018). A Global Empirical Model for Near-Real-Time Assessment of Seismically Induced Landslides. Journal of Geophysical Research: Earth Surface, 123(8), 1835–1859. https://doi.org/10.1029/2017JF004494

Papathanassiou, G. Valkaniotis, S. Ganas, A. & Pavlides, S. (2017). *Earthquake-induced landslides in the island of Lefkada, Ionian Islands, Greece* [GIS data]. Retrieved from the U.S. Geological Survey website: **https://doi.org/10.5066/F79G5K96**.

Polykretis, C., Kalogeropoulos, K., Andreopoulos, P., Faka, A., Tsatsaris, A., & Chalkias, C. (2019). Comparison of statistical analysis models for susceptibility assessment of earthquake-triggered landslides: A case study from 2015 earthquake in Lefkada Island. Geosciences (Switzerland), 9(8). https://doi.org/10.3390/geosciences9080350

Reichenbach, P., Rossi, M., Malamud, B.D, Mihir, M., & Guzzetti, F. (2018). A review of statistically-based landslide susceptibility models. Earth Science Reviews, 180 (2018), 60-91. **https://doi.org/10.1016/j.earscirev.2018.03.001**.

Roback, K., Clark, M.K., West, A.J., Zekkos, D., Li, G., Gallen, S.F., … & Godt, J.W. (2017). *Map data of landslides triggered by the 25 April 2015 Mw 7.8 Gorkha, Nepal earthquake* [GIS data]. Retrieved from the U.S. Geological Survey website: https://doi.org/10.5066/F7DZ06F9.

Rymer, M. J. (1987). *Landslides triggered by the San Salvador earthquake of October 10, 1986* [GIS data]. Retrieved from the U.S. Geological Survey website: **https://doi.org/10.5066/F7BG2MHG.**

Sato, H.P., Hasegawa, H., Fujiwara, S., Tobita, M., Koarai, M., Une, H., & Iwahashi, J. (2017). *Landslide distribution triggered by the 2005 Northern Pakistan earthquake using SPOT 5 imagery* [GIS data]. Retrieved from the U.S. Geological Survey website: https://doi.org/10.5066/F7SJ1J42.

Sekiguchi, T., & Sato, H.P. (2017). *Feature and distribution of landslides induced by the Mid Niigata Prefecture earthquake in 2004 Japan* [GIS data]. Retrieved from the U.S. Geological Survey website: **https://doi.org/10.5066/F7X928TX**.

Shao, X., Ma, S., Xu, C., & Zhou, Q. (2020). Effects of sampling intensity and non-slide/slide sample ratio on the occurrence probability of coseismic landslides. Geomorphology, 363. **https://doi.org/10.1016/j.geomorph.2020.107222**

Tanyaş, H., & Lombardo, L. (2019). Variation in landslide-affected area under the control of ground motion and topography. Engineering Geology, 260. https://doi.org/10.1016/j.enggeo.2019.105229

Tanyaş, H., van Westen, C. J., Persello, C., & Alvioli, M. (2019). Rapid prediction of the magnitude scale of landslide events triggered by an earthquake. Landslides, 16(4), 661–676. https://doi.org/10.1007/s10346-019-01136-4

Trabucco, A. & Zomer, R.J. (2018). Global Aridity Index and Potential Evapo-Transpiration (ET0) Climate Database v2. CGIAR Consortium for Spatial Information (CGIAR-CSI). Published online, available from the CGIAR-CSI GeoPortal at **https://cgiarcsi.community**

Uchida, T., Kataoka, S., Iwao, T., Matsuo, O., Terada, H., Nakano, Y., … Osanai, N. (2017). *Landslides triggered by the January 16, 1995, M 6.9 Kobe, Japan Earthquake* [GIS data]. Retrieved from U.S. Geological Survey website: https://doi.org/10.5066/F7TH8K60.

Wartman, J., Dunham, L., Tiwari, B., & Pradelm, D. (2017*). Landslides in Eastern Honshu induced by the 2011 Tohoku earthquake* [GIS data]. Retrieved from the U.S. Geological Survey website: **https://doi.org/10.5066/F7G73C76**.

Worden, C.B., and Wald, D.J. (2016). ShakeMap Manual, http://dx.doi.org/10.5066/F7D21VPQ

Xu, C., Xu, X., Shyu, J. B. H., Zheng, W., & Min, W. (2014). *Landslides triggered by the July 22, 2013 Minxian - Zhangxin, China, Mw 5.9 earthquake* [GIS data]. Retrieved from the U.S. Geological Survey website: **https://doi.org/10.5066/F7V986KM.**

Xu, C., Xu, X., Shen, L., Dou, S., Wu, S., Tian, Y., & Li, X. (2017). *Inventory of landslides triggered by the 2014 Ms 6.5 Ludian earthquake* [GIS data]. Retrieved from the U.S. Geological Survey website: **https://doi.org/10.5066/F7QJ7FTF**.

Xu, C., Xu, X., & Shyu, J.B.H. (2017). *Database and spatial distribution of landslides triggered by the Lushan, China Mw 6.6 earthquake of April 20, 2013* [GIS data]. Retrieved from the U.S. Geological Survey website: **https://doi.org/10.5066/F7KS6Q2P**.

Xu, C., Xu, X., Yao, X., & Dai, F. (2017). *Landslides triggered by the May 12, 2008, Wenchuan Mw 7.9 earthquake of China* [GIS data]. Retrieved from the U.S. Geological Survey website: **https://doi.org/10.5066/F7RJ4H0P**.

Yagi, H., Sato, G., Higaki, D., Yamamoto, M., & Yamasaki, T. (2009). *Distribution and characteristics of landslides induced by Iwate-Miyagi Nairiku Earthqake in 2008 in Tohoku district, Northeast Japan* [GIS data]. Retrieved from the U.S. Geological Survey website: https://doi.org/10.5066/P9PRGNWR.

Zhang, J., Liu, R., Deng, W., Khanal, N.R., Gurung, D.R., Murthy, M.S.R., & Wahid, S. (2017). *Characteristics of landslides in Koshi River basin, Central Himalaya* [GIS data]. Retrieved from the U.S. Geological Survey website: https://doi.org/10.5066/F73T9FQ1.

APPENDIX A
DETAILED METHODOLOGY

A.1. INTRODUCTION

This appendix provides a detailed description of the methodology used to create and validate a coseismic landslide susceptibility map for Bhutan. It describes the collection of physiographic data associated with landslide events, and the ways in which landslide and non-landslide observations were sampled. It describes the models used, how they were trained, and how the model performance was evaluated. Finally, it shows the quantitative performance of the models across the various landslide events and provides example outputs of the coseismic landslide score maps generated by the models and their translation into susceptibility maps.

A.2. METHODOLOGY

A.2.1. Geospatial Data Collection

A.2.1.1. Coseismic Landslide Inventories

No known inventories of coseismic landslides for earthquakes in Bhutan are currently known to be available. Coseismic landslide inventories from around the world were compiled to capture as broad of a physiographic setting as possible. These inventories consisted of polygon or point geometries delineating the locations of mapped landslides associated with specific earthquake events. The methodologies employed in the creation of the inventories and the level of completeness was thought to vary across each inventory. For instance, in some inventories it was clear that only landslides visible from road-based reconnaissance were identified, whereas in other inventories it appeared that remote sensing imagery and potentially computer vision-based classification were used. The result is that the latter would be expected to offer more comprehensive coverage of the entire landslide population as compared to the former, which would be biased to landslides that occurred near roads (and therefore physiography conducive to roadbuilding and to anthropogenic contributors due to improved accessibility) and omitted landslides further into mountainous terrain. An additional limitation of some of the inventories was that the date of the event was so far in the past that current physiographic data may no longer be consistent with the environment in which the original landslides occurred. Table A-1 summarizes the coseismic databases used for this study.

Table A-1. Summary of coseismic landslide inventories considered within this study.

Event Location	Date	Magnitude	LS Data Type	Number of Observations	Reference
Lorca, Spain	May 11, 2011	5.1	Points	166	Alfaro et al. (2012)
San Salvador, El Salvador	October 10, 1986	5.7	Points	268	Rymer, 1987
Minxian-Zhangxian, China	July 21, 2013	5.9	Polygons	2330	Xu, Xu, Shyu, et al. (2014)
AysenFjord, Chile	April 21, 2007	6.2	Polygons	517	Gorum et al. (2014)
Ludian, China	August 3, 2014	6.2	Polygons	1024	Ying-Ying et al. (2015)
Abruzzo, Italy	April 6, 2009	6.3	Polygons	89	Piacentini et al. (2013)
Lefkada, Greece	August 14, 2003	6.3	Polygons	274	Papathanassiou et al. (2013)
Friuli, Italy	May 5, 1976	6.5	Points	1007	Govi 1977
Niigata-Chuetsu, Japan	October 23, 2004	6.6	Polygons	4615	Sekiguchi and Sato (2006)
Lushan, China	April 20, 2013	6.6	Polygons	15546	Xu et al. (2015)
San Fernando, California	February 2, 1971	6.6	Points	391	Morton, 1971
El Salvador	February 13, 2001	6.6	Points	62	Ministerio de Medio Ambiente y Recursos Naturales, El Salvador (2017)
KiholoBay, Hawaii	October 15, 2006	6.7	Polygons	383	Harp et al. (2014)
Coalinga, California	May 2, 1983	6.7	Polygons	3980	Harp and Keefer 1990
Northridge, California	January 17, 1994	6.7	Polygons	11111	Harp and Jibson (1996)
Kobe, Japan	January 16, 1995	6.9	Polygons	2353	Uchida et al. (2004)
Iwate-Miyagi-Nairuku, Japan	June 14, 2008	6.9	Polygons	4211	Yagi et al. (2009)
Loma Prieta, California	October 17, 1989	6.9	Points	528	Keefer and Manson (1998)
Haiti	January 12, 2010	7	Polygons	23567	Harp et al. (2016)
Guatemala	February 4, 1976	7.5	Polygons	6224	Harp et al 1977
Kashmir, Pakistan	October 8, 2005	7.6	Points	2424	Sato et al. (2007)
Chi-Chi, Taiwan	September 20, 1999	7.7	Polygons	9272	Liao and Lee (2000)
Denali, Alaska	November 3, 2002	7.9	Polygons	1579	Gorum et al. (2014)
Wenchuan, China	May 12, 2008	7.9	Polygons	197481	Xu, Xu, Yao, et al. (2014)
Tohoku, Japan	March 11, 2011	9.1	Polygons	3477	Wartman et al. (2013)
Gorka, Nepal	April 25, 2015	7.8	Points/Polygons	450921	Gnyawali et al (2016); Roback et al (2017); Zhang et al (2016)

A.2.1.2. Physiographic Variables

To build a coseismic landslide susceptibility model it was necessary to collect information about the environment in which the landslides occurred. Various types of supplementary geospatial data were collected for the areas in the vicinity of each of the coseismic landslide events, where the vicinity for each event was defined as the extent of the associated United States Geological Service (USGS) Shakemap. The data collected for each event are shown in Table A-2. These variables were chosen based on knowledge of landslide mechanics and the availability of datasets at a global scale. Most of the chosen parameters have been used in previous studies reviewed for this work, including that of Nowicki Jessee et al. (2018).

Table A-2. A summary of data collected considered for use as explanatory variables in the coseismic susceptibility model.

Category	Variable	Data Type	Source	Spatial Resolution
Seismic Derivatives	Peak Ground Acceleration (PGA)	Continuous raster	USGS Shakemap System (Worden & Wald, 2016)	1 km
	Peak Ground Velocity (PGV)			
	Modified Mercalli Intensity (MMI)			
Topographic Derivatives	Elevation	Continuous raster	Shuttle Radar Topography Mission (SRTM) Digital Elevation Model (DEM)	30 m
	Slope Angle			
	Relative Slope Aspect[1]			
	Local Relief			
	Curvature (plan, profile, combined)			
	Compound Topographic Index			
Precipitation	Average Annual Precipitation	Continuous raster	WorldClim Mean Monthly Precipitation	30 arc-seconds
Aridity	Annual average reference evapotranspiration	Continuous raster	Trabucco and Zomer (2018)	30 arc-seconds
	Annual average aridity index			
Vegetative cover	Percentage green vegetation cover	Continuous Raster	Broxton, Zeng, Scheftic, and Troch (2014)	30 arc-seconds

Category	Variable	Data Type	Source	Spatial Resolution
Lithology	GLiM Global Lithology Data	15-class categorical vector	Hartmann and Moosdorf (2012)	Extracted from a vector dataset (approximately 1:1,000,000 scale)
Landcover	Globecover 2009 Landcover	20-class categorical raster	Arino et al. (2012)	300 m

Note:

1. Relative slope aspect combined topographic data with earthquake location information and is therefore a partial function of the earthquake event, unlike the other non-seismic datasets

A.2.2. Data Extraction for Landslide Observations

After the explanatory variables had been collected for each of the landslide event areas, BGC spatially associated each of the landslide observations with the explanatory variables (i.e., positive samples at landslide locations). This was done by either extracting the value of each raster dataset at the centroid of each landslide, or in the case where the landslide geometry was provided as a point, at the landslide point. The landslide inventories only mapped where landslides occurred and did not include any information about where landslides did not occur. Therefore, a method was developed to obtain samples of the landslide vicinity where no landslide occurred (i.e., negative samples). Numerous methods were explored to generate these negative samples for each event. In general, they included the following differences:

a. Looking either within the bounds of the mapped landslides or within the bounds of the Shakemap.
b. Sampling using a uniform random distribution within the selected bounds, or a non-uniform random distribution with a probabilistic tendency to sample near the center of mapped landslide inventory (i.e., lower sample density with distance from the centre of the landslide inventory). One such approach involved inverse distance weighted (IDW) of sample distribution.

All random samples that were within 385 m[1] of a mapped landslide were discarded as potential negative samples, and a subset of the random samples were randomly chosen such that the number of non-landslide samples equaled the number of landslide samples. This process was repeated for each of the landslide inventories. Examples are shown in Figure A-1.

Each of the sampling techniques exhibited various trade-offs. Models with sampling done randomly across the entire Shakemap demonstrated the best accuracy metrics. However, these high metrics were potentially misleading because the model was able to use Shakemap variables to predominately separate landslide from non-landslide observations. As such these models had high error in the vicinity of the landslide inventory, which by the nature of the sampling technique

[1] This distance was adopted from Nowicki Jessee et al. (2018), which was the value they found to be the 95th percentile of the distance between centroids of the landslides in their inventories.

only constituted a fraction of the total sample space. Conversely, models with samples taken from within the landslide inventory bounds showed the poorest accuracy metrics. This is believed to be because given the extent of the inventories and the resolution of the underlying data, for every positive sample there was very likely to be a negative sample with nearly the same physiographic characteristics. As a result, the model tended to be unable to separate the landslide (positive) samples from the non-landslide (negative) samples with high predictive power. The IDW sampling regime was conceived in efforts to merge the two approaches: it samples widely across the Shakemap to sample the full range of Shakemap parameter values but places samples more densely towards the landslide inventory to force the model to learn to distinguish between landslides and non-landslides in highly seismic areas. A maximum of 20,000 landslides were used from each inventory. If the number of landslides in the inventory exceeded 20,000, a subset of all landslides was chosen at random.

A.2.3. Model Selection

Two types of machine learning model algorithms were explored in this work for the development of production models: logistic regression (LR) and light gradient boosted machines (LGBM). A third model, the weights of evidence (WoE) method was also used, primarily to assist in trouble shooting, model validation and parameter sensitivity testing.

A.2.3.1. Logistic Regression

Logistic regression is a machine learning model often employed for classification problems, particularly for binary classification (i.e., when the target variable takes on a value 0 or 1). The model takes on the form in equation [1]:

$$P(y = 1|X) = \frac{1}{1 - e^{-\theta^T X}} \quad [1]$$

Where:

$$\theta^T X = \beta_0 + \sum_{i=1}^{n} \beta_i x_i \quad [2]$$

Where:

β_0 = The model intercept

β_i = The model parameter for variable i with value x

The output of this model represents the probability of the target variable given the input vector X. The form of this model is similar to that of a multivariate linear regression, with the main differences being that the output is a probability and that predictions scale multiplicatively with changes in inputs or parameters rather than additively. Logistic regression is a widely used model in many fields including the prediction of coseismic landslides (e.g., Nowicki Jessee et al., 2018). Its benefits include that it is relatively simple and interpretable, but its main drawback is that it cannot capture non-linear interactions between variables without explicit feature engineering.

A.2.3.2. Light Gradient Boosted Machines

Light Gradient Boosted Machines are a regression tree-based machine learning model that relies on gradient boosting to build new estimators. The model takes on the form in equation [3]:

$$P(y = 1|X) = \sum_{k=1}^{K} f_k(X) \qquad [3]$$

Where:

K = The number of regression tree estimators and X is the input variable vector.

Each estimator function f_k is a weak regression tree that makes predictions by iteratively making splits on input values. In gradient boosting, new estimators are added and trained on the errors of the preceding tree. This process is repeated until the model consists of a series of weak learners that together provide a model with more predictive power than a single decision tree. Due to the presence of numerous trees making numerous splits, this model can capture non-linear interactions between input variables without specifying them explicitly. This family of models has been successfully applied to a variety of problems across many fields. Its main drawback is that it is relatively easy to overfit the model and the proper specification of hyperparameters is important.

A.2.3.3. Weights of Evidence

A modified approach to the weights of evidence method (Bonham-Carter et al., 1989) was used as the main framework to develop a coseismic landslide susceptibility map for QA and testing purposes. The WoE method is a bivariate statistical approach; this means that landslides are compared statistically with each thematic map, one at a time, and individual relationships are subsequently combined. The method combines features of various thematic maps expected to have some relationship to the presence or absence of landslides. Weights are calculated for each thematic map based on the conditional probability (P) of the presence or absence of a landslide given the presence of the theme, and these individual weights are combined to develop an overall weight map.

The individual thematic positive weights (Wi) are calculated by taking the logarithm of the ratio of spatial probabilities, shown in equation [4], below. The weights are combined through simple addition, which is mathematically equivalent to multiplication of the ratios of probabilities as per equation [4].

$$W_i = \log\left[\frac{P(F_i|L)}{P(F_i|\bar{L})}\right] \quad [4]$$

Where:

W_i = The positive weight for the ith thematic factor

F_i = The presence of the ith thematic factor

L = The presence of a landslide

$\bar{L}$ = The absence of a landslide

and $P(F_i|L)$ is the probability of F_i given L

In the geographic information systems (GIS) environment, the spatial probabilities in equation [4] are calculated by summing the number of raster pixels where landslides are present or absent and where a specific factor is also present. Equation [4], using GIS raster algebra, hence becomes equation [5], below.

$$W_i = \log\left[\left(\frac{A_1}{A_2}\right) / \left(\frac{A_3}{A_4}\right)\right] \quad [5]$$

Where:

A_1 = The area within the specific factor containing landslides

A_2 = The total area within the analytical study area containing landslides

A_3 = The area within the specific factor not containing landslides

A_4 = The total area within the analytical study area not containing landslides

and the analytical study is the area within which landslides have been completely mapped.

This approach was modified for the present study, which used random samples of raster values from the whole map and associated raster values at every inventoried landslide location.

The weight values are calculated within a specific point, or map pixel, where the ith theme (say, soil type) has a specific value. The A_i values and calculated weight are the same at any other point on the map with the same thematic value, and therefore the number of different weight values for W_i depends on the number of different thematic values (e.g., number of different soil types).

Landslide susceptibility is obtained by combining the thematic weights, W_i, to obtain an overall combined weight, as shown in equation [6].

$$W_{total} = \sum_{i=1}^{n} W_i \quad [6]$$

The combined map will have numeric values ranging between low (highly negative) and high (highly positive) values, where higher values represent a higher spatial probability of landslide presence. The numeric range in this combined map can be reclassified or subdivided into smaller ranges representing, for example, high, medium and low susceptibility. Some degree of testing is usually required to allow the map values to be translated into practical meaning.

Some variations were made from strict application of the weights of evidence method:

1. W_i described in equation [4] above is the "positive weight" and the formal weights of evidence method also includes consideration of negative weights. Positive weights, W_i, indicate a positive relationship between the presence of a factor and landslide presence, while negative weights indicate a negative relationship between factor and landslide presence. In the author's experience, inclusion of the negative weights adds little or no information or predictive value to the model, and so they were omitted from the work.
2. In the standard weights of evidence approach, thematic weight maps are combined through direct addition to produce the overall susceptibility map. This approach presumes that the various thematic maps considered for inclusion are independent of each other. In practice, the various themes are usually correlated to some degree, and better predictive power can be obtained by adjusting the value of included weight maps in the model. For example, slope angle may be more informative than land use class, and better predictive power may be obtained by giving the slope weight map more importance in the final map. The map is optimized through trial and error, considering a wide range of combinations to find best predictive power.
3. The principle of parsimony is applied by seeking to minimize the number of explanatory variables included in the final model. Themes are excluded from the final model if they add little predictive power, as determined by considering the Receiver Operating Characteristic Area Under the Curve (RoC AUC) with and without their inclusion.
4. Rather than wholly or randomly sampling non-landslide areas to compare with the full set of landslide points, the whole map area was sampled. This approach includes some true positives (i.e., landslides) in the comparative dataset, which can diminish the explanatory value of the map values in the resulting analysis. In practice, the resulting error is very small if the total fraction of map area occupied by landslides is small. For example, if 1% of the map area is occupied by landslides, then any randomly selected point has a 99% probability of being a true negative (i.e., not a landslide), which is not substantially worse than would be the case when sampling map areas outside inventoried landslides, since no inventory is complete and accurate.
5. Landslides and random map areas were not sampled with equal spatial density, such that the ratios of true positives to presumed true negatives (i.e., random points from the map) do not represent spatial probabilities as shown in equations [4] and [5]. However, the overall ratio is proportional to the spatial probability and the error it introduces can be accounted for in the spreadsheet analysis. As a result, however, the map output should be considered as a relative susceptibility score, indicative of higher and lower probability, but not a direct measure of probability.

These variations from the strict approach of Bonham-Carter et al. (1989) create mathematical differences from the theoretical approach but they do not affect the value of the resulting analysis. The basic assumption of independence between explanatory variables is never fully met and that introduces greater potential to vary from the theoretical expectation, in our experience. The value of the analytical result is tested through validation trials and does not depend solely on the theoretical expectation from the strict formulation.

In addition to producing an index estimate of landslide susceptibility, it is also possible to transform the map values to represent the expected number of landslides per area. This is obtained by dividing the total number of landslides sampled from all event databases (283,405) by the total area of all event Shakemaps (6,772,000 km^2) to obtain an overall average of 0.04185 observed landslides per km^2, or 1.09 landslide points per random point used in the weights of evidence analysis. The calculated weight values can be reclassified based on the number of landslide points versus random points (presumed true negatives) within a given range, recognizing that each of the 259,986 random samples across all Shakemaps represents 26.05 km^2 of map area (i.e., 6.77 million km^2 ÷ 259,986 points). For any arbitrary range of weight values constraining X landslide points and Y random points in the map, the expected landslide density is therefore X / [Y x 26.05 x 1.09]. For example, the weight values of 4.80 to 5.31 contain 78 random points, representing 2031.9 km^2, and 28,207 landslide points, giving an expected landslide frequency of 12.74 landslides per km^2.

A.2.4. Feature Transformation

Feature transformation is the process to transform input data to help a model draw more information from it. This is important because not all input data is suitable for model training as-is. The following feature transformation steps were taken during model development prior to training the model:

1. For the LR model, all categorical features were one-hot-encoded, meaning if a sample had a particular lithology, the lithology corresponding to that variable would obtain a value of 1 and the value for all other lithology variables received a value of 0. This transformation was applied to landcover features as well as lithological features.
2. In the LR model, all non-categorical features were scaled to obtain a mean of zero and variance of 1. This was done to comply with the assumption of the L2 regularization[2] routine employed in the LR training process. Non-categorical features were not scaled in the LGBM model.
3. For the LGBM models, categorical features were not one-hot-encoded. Instead, they were given a number between 1 and 15 (lithology) or 1 and 20 (landcover). The categorical features were passed separately to the model and the model treated them differently than the continuous variables.

[2] L2 regularization is an approach applied to the loss function in a machine learning algorithm that penalizes large weights. It is employed to address model overfitting.

4. For curvature, profile curvature, and plan curvature, the absolute value was usually taken. This was to reflect the fact that deviation from a flat plane rather than specifically concavity or convexity may be associated with landslides. In the WoE model, both absolute values and original values were considered, allowing a check on the importance of concavity versus convexity in model power.
5. The natural logarithms of the mean predicted PGV and PGA were used, as this is what was provided in the USGS Shakemaps.

A.2.5. Model Training and Validation

The output of the data extraction step was a table containing landslide and non-landslide points for each event, along with the values of the explanatory variables at those locations. These data were used to train a model to derive the numerical relationship between the explanatory variables and the presence or absence of landslides. Numerous LR and LGBM models were created that differed in the following categories:

1. Sampling regime.
2. Selected input variables.
3. Model type.
4. Feature engineering differences.

The choice of the four settings constituted a unique trial. For each trial a k-fold[3] validation was completed. This involved creating n-2 folds (n = number of landslide-producing earthquake events, n-2 = k), where each fold had a randomly selected group of n-2 events in the training data, a common event as the test data, and the remaining event as the validation data. This allowed for evaluation of the model on each event such that the model under consideration was validated on an event it had not been trained on, for a total of n-2 models.

For each type of model, various hyperparameter optimizations were completed using the Tree Parzen Estimator method. The hyperparameter search spaces used for each model type are shown in Table A-3. During hyperparameter optimization, the loss function L was defined according to equation [7]:

$$L = \frac{\sum_{k=1}^{n-2}(1 - F_{0.5}(k))}{n-2} \qquad [7]$$

Where:

k = the fold number

n is the number of events

$F_{0.5}(k)$ = the F-score of a model trained on fold k using a decision threshold of 0.5.

[3] A fold is a single random division of all available observed data into a training data subset, a validation data subset, and sometimes also a test data subset. In k-fold validation this random division process is completed k times to obtain k folds.

This equation shows that the hyperparameters were chosen to optimize the average F-score at a 0.5 decision threshold across all validation events across all folds. The four hyperparameter sets with the lowest loss were tested and the models with the results qualitatively judged to be most appropriate were selected for use.

Table A-3. Hyperparameter search space for each model type.

Model	Hyperparameter Name	Range
Logistic Regression[1]	Regularization strength	[1 x 10^{-4}, 1 x 10^{4}]
	Fit Intercept	[True, False]
	Solver	[lbfgs, liblinear]
Light Gradient Boosted Machine[2]	Number of leaves	[2, 2^{12}]
	Learning rate	[0.01, 0.1]
	Number of estimators	[2, 2^{10}]
	Max tree depth	[2, 12]

Notes:

1. Documentation for this implementation and a description of the meaning of the hyperparameters is available here: https://scikit-learn.org/stable/modules/generated/sklearn.linear_model.LogisticRegression.html.
2. Documentation for this implementation and a description of the meaning of the hyperparameters is available here: https://lightgbm.readthedocs.io/en/latest/pythonapi/lightgbm.LGBMClassifier.html.

For a given hyperparameter set, n-2 models were created, and the F-score and RoC AUC score were recorded to evaluate performance and determine at which decision threshold the optimum F-score was obtained for each validation event. Each model was then evaluated using set decision thresholds and the balanced accuracy BA was calculated according to equation [8]:

$$BA = \frac{1}{2}\left[\left(\frac{TP}{S_P}\right) + \left(\frac{TN}{S_N}\right)\right] \qquad [8]$$

Where:

TP = the number of true positives

S_P = the number of positive samples

TN = the number of true negatives

S_N = the number of negative samples

The balanced accuracy scores across all models in the fold set were used to quantitatively evaluate the model performance on unseen data by selecting for models that had the most events with a balanced accuracy greater than or equal to 0.9. A final model using all n events in the training data was then trained using the same hyper parameters, and the output was qualitatively evaluated to check for geospatial and logical consistency. The settings obtained for the final LGBM model are shown in Table A-4 and inferred parameter importance based on the number of splits in the trees in that model is shown in Table A-5. The settings obtained for the final LR model

are shown in Table A-6 and inferred parameter importance based on the parameter weights is shown in Table A-7.

Table A-4. Settings for final LGBM model.

Sampling regime	Partially random inverse distance weight power of 5	
Input variables	• logPGV • logPGA • lithology (15 classes) • landcover (20 classes) • curvature • plan curvature • profile curvature • 3-cell local relief • 15-cell local relief • 30-cell local relief • slope	
Model type	LGBM	
Feature transformations	curvature	absolute value
	plan curvature	absolute value
	profile curvature	absolute value
Hyperparameters	Estimators	500
	Leaves	32
	Max depth	5
	Learning rate	0.015

Table A-5. Parameter importance for final LGBM model.

Parameter name	Long name	Importance (based on number of splits)
pga_mean	mean logPGA	3108
pgv_mean	mean logPGV	2167
lithology	lithology	2057
lr_30cell	30 cell local relief	1652
landcover	landcover	1635
lr_3cell	3 cell local relief	1539
lr_15cell	15 cell local relief	934
slope	slope	623
pr_curve	profile curvature	481

Parameter name	Long name	Importance (based on number of splits)
pl_curve	plan curvature	325
curv	curvature	254

Table A-6. Settings for final LR model.

Sampling regime	Partially random inverse distance weight power of 5	
Input variables	• logPGV • logPGA • lithology (15 classes) • landcover (20 classes) • curvature • plan curvature • profile curvature • 3-cell local relief • 15-cell local relief • 30-cell local relief • slope	
Model type	LR	
Feature transformations	curvature	absolute value
	plan curvature	absolute value
	profile curvature	absolute value
	all features	scaled by mean and variance
Hyperparameters	Fit intercept	False
	Solver	lbfgs
	Regularization strength	2.2×10^{-4}

Table A-7. Parameter contributions for final LR model.

Name	Value
logPGV	3.43E-01
logPGA	3.37E-01
Slope	1.15E-01
3-cell local relief	1.08E-01
15-cell local relief	7.45E-02
30-cell local relief	5.71E-02
Profile curvature	5.01E-02

Name	Value
Plan curvature	4.80E-02
Curvature	4.47E-02
Average annual precipitation	2.06E-02
Closed needleleaved evergreen forest	2.00E-02
Basic volcanic rocks	1.96E-02
Closed to open mixed broadleaved and needleleaved forest	9.33E-03
Siliciclastic sedimentary rocks	5.94E-03
Mosaic cropland	3.49E-03
Intermediate volcanic rocks	2.99E-03
Acid volcanic rocks	2.96E-03
Acid plutonic rocks	1.58E-03
Carbonate sedimentary rocks	1.45E-03
Closed to open herbaceous vegetation	1.27E-03
Pyroclastics	1.23E-03
Sparse vegetation	9.46E-04
Ice and glaciers	1.93E-04
Closed broadleaved deciduous forest	4.72E-05
Open broadleaved deciduous forest/woodland	3.64E-05
Closed to open broadleaved forest regularly flooded	1.27E-05
Evaporites	-1.59E-06
No data	-4.15E-06
Mosaic forest or shrubland/grassland	-1.54E-05
Closed to open grassland or woody vegetation on regularly flooded or waterlogged soil fresh brackish or saline water	-2.13E-05
Closed to open broadleaved evergreen or semideciduous forest	-2.29E-04
Intermediate plutonic rocks	-2.47E-04
Basic plutonic rocks	-2.63E-04
No data	-3.87E-04
Metamorphics	-6.63E-04
Water bodies	-7.44E-04
Mosaic grassland/forests or shrubland	-7.84E-04
Open needleleaved deciduous or evergreen forest	-1.06E-03
Bare areas	-1.78E-03
Artificial surfaces and associated areas	-1.87E-03

Name	Value
Permanent snow and ice	-2.27E-03
Closed to open broadleaved or needleaved evergreen or deciduous shrubland	-3.40E-03
Mixed sedimentary rocks	-7.43E-03
Mosaic vegetation	-7.70E-03
Rainfed croplands	-1.27E-02
Unconsolidated sediments	-2.84E-02

Calculated weight values used in the WoE model have not been included in this report but can be provided on request. The parameters included in the final models, along with their assigned contribution to the models, and shown in Table A-8.

Table A-8. Parameter contributions for final WoE models.

Model Parameter		Contributions	
Name	**Description**	**Full Model**	**PGA Only Model**
pga_mean	Mean value of ln(PGA) obtained from the USGS Shakemap	1	2.5
pgv_mean	Mean value of ln(PGV) obtained from the USGS Shakemap	1	0
mmi_mean	Mean value modified Mercalli intensity obtained from the USGS Shakemap	0.5	0
ai_et0	Average annual aridity index	1	1
et0_yr	Average annual evapotranspiration	0.5	0.5
Average	Proportion of green vegetation	1	1
Land cover	Land cover	0.5	0.5
Slope	Slope angle from 30 m SRTM DEM[1]	0	0.5
lr_3cell	3 cell (90 m) local relief from 30 m SRTM DEM	1.5	1
lr_30cell	30 cell (900 m) local relief from 30 m SRTM DEM	0.5	0.5
lr_300cell	300 cell (9000 m) local relief from 30 m SRTM DEM	0.5	0.5

A.2.6. Inference

The model was trained on tabular data that originated from landslide points extracted on raster data. To produce a raster predictive map, the model had to use raster data as input. To run inference on a model, the DEM for the event of interest was used as the base raster. All other features that were not derived from the DEM were then resampled to the resolution of the base DEM (~30 m). Continuous rasters were interpolated using bilinear interpolation, and categorical rasters were interpolated using nearest neighbour interpolation. All necessary feature

transformation steps were applied to the raster data, and it was flattened into a tabular structure suitable for input into the model. The model was run using this data, which was then reshaped into the original raster array size and written to a tif file.

Due to various factors regarding experimental design and fundamental aspects of the approach, the outputs of the models do not directly represent the probability that a particular cell will experience a landslide. The outputs of the models are instead scores that must be modified to account for landslide occurrence associated with various score values to translate the output into susceptibility. The process by which this is done is explained in Section A.2.3.3.

A.2.7. Validation of Results

There are no coseismic landslide inventories available for Bhutan, and so the model could not be validated directly for Bhutan. As the best approximate proxy, the magnitude 7.8 earthquake that occurred in Nepal on April 25, 2015 was selected (the 'Gorkha' event). This event was left out of all model training, validation, and testing steps. The accuracy of the model as applied to this case is thought to be the best approximation for how the same model could perform for an earthquake occurring in Bhutan given the model had not included any Bhutanese or Nepalese data during training.

A.3. RESULTS AND DISCUSSION

The results of the susceptibility modelling can be broken down into two types of analyses. The first deals with the model performance on the global datasets used to create the model. The second deals with the interpretation of the susceptibility model itself as a predictor for an earthquake not seen in model training. Finally, the coseismic landslide susceptibility map for Bhutan is shown for the M7 scenario earthquake in in Drawing 001 and for the M8 scenario earthquake in Drawing 002.

A.3.1. Quantitative Performance of the Coseismic Landslide Models on Global Datasets

Figure A-2 and Figure A-3 depict balanced accuracy metrics for the LGBM and LR coseismic landslide models evaluated across all 23 folds used in the k-fold validation. The balanced accuracy metric is calculated for both the decision threshold that maximizes the F-score for each validation event and a decision threshold of 0.5. Balanced accuracy is used to evaluate model performance because it gives equal weight to true positive (TP) rates and true negative (TN) rates and is also easier to interpret than F-score. The use of balanced accuracy reflects the idea that we are interested in correctly identifying landslides while also not mis-classifying non-landslides. The use of balanced accuracy also allows for comparison against the model proposed in Nowicki Jessee et al. (2018).

Overall, the models demonstrate skill in differentiating between landslide and non-landslide events. Evaluation of the LGBM model shows that 14 of 23 events have a balanced accuracy > 90% at some decision threshold, and 20/23 events have a true positive rate of > 90%. For the LR model, 14/23 events have a balanced accuracy > 90% at some decision threshold, and all

23 events have a true positive rate of > 90% at their best decision thresholds. At a universal decision threshold of 0.5, the skill of both models decreases on average across the entire set of events but still shows respectable skill for many events. Notable is the poor performance for the 2011 Spain M5.1, 2013 China M5.9, and 2001 El Salvador M7.7 events, which show poor true positive rates. This means that the model tends to predict that landsliding points are not landslides at a decision threshold of 0.5, and that better balanced accuracy metrics are only achieved at a lower decision threshold.

Examining these three events in more detail reveals something about why the model may perform poorly for these landslide inventories. One aspect that these three events had in common was that their seismicity features (logPGA and logPGV) were lower on average compared to the training data for their respective folds, and the distributions of these features with respect to landslide and non-landslide points did not align well with the training data. This is demonstrated in Figure A-4. Figure A-5 shows that the optimum decision threshold tends to increase with increasing seismic load expressed as logPGA. This relationship between optimum decision threshold and seismicity highlights how the inclusion of logPGA and logPGV can be challenging to do correctly. In many of the landslide inventories across the training set, there are non-landslide samples with logPGA and logPGV values that are higher than the logPGA and logPGV values of landslide samples from the 2011 Spain M5.1, 2013 China M5.9, and 2001 El Salvador M7.7 landslide inventories. The model has learned that higher seismicity values tend to be associated with landslides, and so for landslide inventories associated with relatively low seismic activity relative to the entire compiled dataset, the predicted landslide score is low. However, the predictive skill of the model can be increased if the decision threshold is decreased for these cases.

One might wonder why this notion applies to the 2001 El Salvador M7.7 event given that such a large earthquake is on the higher end of the event magnitudes included in the inventory. While the magnitude was high, the seismicity of the area experiencing landslides was relatively small since the epicenter was located offshore. Additionally, a proportion of the randomly selected non-landslide points had higher seismicity than the landslide points but were not shown to have experienced landslides due to either incomplete inventories or other factors not included in the model such as proximity to a fault. Generally, it was seen that the optimum decision threshold for a given event was proportional to the median logPGA of the landslide samples (Figure A-5), and most events were well modelled at some decision threshold that differed based on the nature of event and local conditions.

Given the broad variety of landsliding environments, quality of inventories, and representation in the datasets, it is not unexpected that the model does not perform equally across all geographies at a given decision threshold. A model that performs equally well for all events at a given threshold is desirable since it means that the probabilities are directly translatable across geographies. The balanced accuracy scores here indicate that this model is not capable of providing a universally useful decision threshold. However, given that the results show that there tends to be a decision

threshold that works well for almost all events, the model outputs can still provide value in a local context if the probabilities are translated into local meaning.

A.3.2. Qualitative Performance of the Coseismic Landslide Models on Global Datasets

Quantitatively, the performance of the LGBM and LR models are similar, but upon inference and subsequent generation of a map, numerous differences in the model outputs become evident. Figure A-6 and Figure A-7 depict predicted landslide probabilities for the 2010 M7.0 event in Haiti for the LGBM and LR models respectively to demonstrate the initial spatial outputs of each model. In a leave-one-out validation test, the LGBM scores a balanced accuracy of approximately 0.90 on the Haiti event, whereas the LR model scored approximately 0.88. However, for the same geographical extent, the LGBM model predicts that much more of the map is expected to contain landslides, and there is a central 'halo' where probabilities are consistently > 0.9. This halo captures many of the observed landslides, but there are also many areas with a high landslide score where no landslides were observed (false positives). This is because these regions have very similar topographic, lithographic, landcover, and seismic features compared to nearby areas where landslides were observed. The same halo region is not as pronounced in the LR model, and there is a clearer distinction between the regions within the halo where landslides were observed and regions where landslides were not observed.

For both models, outside of this main halo region and to the south and west of the map, there are many strips of high score which align well with the inventory. There are instances of false positives and false negatives in both models, but generally higher probabilities are associated with landslide events. Where the models deviate most substantially is in the low-lying urban area to the northwest of the halo highlighted in Figure A-8. The LGBM model predicts very low chance of landsliding in this region, predominantly because the area is quite flat (refer to Figure A-8). However, this area has the highest seismicity, and the LR model, being linear, predicts that there is a larger than expected landslide score in this area. The LR model weights the logPGA and logPGV parameters the highest, and so even though the score is reduced by low values for the topographical features, very high seismicity values cause the resulting score to be unrealistically high. The non-linear decision mechanism of the LGBM model allows it to correctly identify that there should be no landsliding in this flat region, even though the seismicity is high. This allows the LGBM model result to be less tied to the patterns of the Shakemap and to eliminate regions more accurately where landsliding should not occur, and more confidently identify landslides further away from the area of highest shaking, such as in the southwest. This appears to come at the cost of a somewhat higher overall predicted score and a more discontinuous score gradient.

A.3.3. Comparison of Machine Learning and Standard Statistical Approaches

Our intent was to apply machine learning methods for this work, including initial focus on the LR method used by Nowicki Jessee et al. (2018). As discussed earlier, we expanded the work to consider other analytical models, ultimately finding both LR and LGBM to give good results. Both methods were implemented using routines written in Python and executed on large computing servers. This configuration provides a powerful basis for computations with very large datasets.

The benefit of fast computations is offset to some degree by greater difficulty tracing the detailed logic and probing the models for sensitivity to specific inputs.

We applied the weights of evidence (WoE) method, first described by Bonham Carter et al. (1989) and commonly applied in landslide susceptibility mapping, as an independent test of the machine learning models. The WoE method is considerably more flexible than other statistical regression methods, as relationships between explanatory data and landslides can be defined arbitrarily without the need to match natural functions like straight lines used in linear regression methods and sigmoid functions used in LR methods. Rather, the range of values for a continuous explanatory variable can be subdivided into specific ranges and associations assigned independent of those for adjacent bins. While this flexibility makes the WoE method potentially more powerful than others fixed to continuous functions, it can also be easier to overfit data. Nevertheless, the method is easily executed in a spreadsheet or simple programming that can be traced and explored. It therefore provides a basis for carefully exploring the logic and testing various inputs for model sensitivity.

Comparative results for the LR, LGBM and WoE models are presented in the following sub-sections; in summary, the LR and LGBM models give broadly similar results to the WoE method. Given our confidence in the WoE method from extensive prior use in practice, we are therefore very confident in the general validity of the LR and LGBM models.

In addition to the models already mentioned, we also combined the LR, LGBM and WoE models, assigning equal weight to each, to develop an ensemble model. This was done by rescaling the three models based on comparative performance for the Nepal earthquake, discussed shortly, and adding them. In the special case where we developed a model excluding PGV, also discussed shortly, we produced a similar ensemble of two models: LR and WoE.

The following sub-sections discuss various results for a range of models applied to several different earthquake events and scenarios, starting with validation cases in Haiti and Nepal and working toward predictions for Bhutan.

A.3.4. M7.0 Haiti Earthquake of 2010

Several models were tested for the 2010 Haiti earthquake in relation to landslides from the event mapped by Harp et al. (2016). This included the two primary machine learning models (LR and LGBM), WoE and the ensemble model with equal contributions from the LR, LGBM and WoE models. These were compared with three model results available from USGS, including Godt et al. (2008), Nowicki et al. (2014) and the USGS' preferred model of Nowicki Jessee et al. (2018). An additional LR model was run excluding PGV and instead using only PGA as a seismic input; that model was included to test models for application to the available Bhutan earthquake scenario PGA models, discussed in Section A.4.

Receiver operating characteristic (RoC) curves are used commonly in the evaluation and comparison of predictive model performance. Curves are shown for the various tested models in Figure A-9. Curves that approach closer to the upper left corner of the RoC graph capture a higher

proportion of actual landslides within a smaller area, and therefore have better predictive power. A random guess with no predictive power would be represented by a diagonal line lower left to upper right. All models have some predictive power; by inspection, the LGBM model had the best performance relative to mapped landslides for this event, with the ensemble model next best. The three USGS models have weaker performance than all five BGC-generated model results in this case.

Qualitative performance as judged by the shape and position of the RoC curve can be quantified by calculating its integral over the full range of false positive rate (i.e., the x axis) from 0 to 1. This provides the “area under the curve” (AUC) which is a simple metric often used to provide a convenient basis for quick comparison of model performance. AUC values for the various models’ RoC curves in Figure A-9 are provided in Table A-9. Those results show that LGBM has the best predictive power, followed by the ensemble model. The two LR models, both with and without PGV, have similar performance, and the WoE model is weakest among all BGC models. The best USGS models in this case are those of Nowicki Jessee et al. (2018) and Nowicki et al. (2014), with both having meaningfully lower performance than the best BGC models.

It is important to recognize that the shape of the RoC curves and associated AUC is sensitive to the model space considered in the comparison. We have used an area extending several kilometers around the limits of mapped landslides. If we consider the whole area of the associated Shakemaps and resulting landslide susceptibility models, we obtain much higher AUC values, approaching 95% or higher. The difference is due to the inclusion of a large additional area of the map where absence of landslides is known with very high confidence, changing the proportion of true positives and false positives across the map. In other word, actual landslides (i.e., true positives) will be constrained within a much smaller area of the map, whereas the outer parts of the map can have some proportion of false positives. The selection of area for model testing does not affect the relative performance of the models.

Table A-9. Model comparison for the 2010 Haiti M7.0 earthquake.

Model		RoC AUC
BGC Models	Ensemble (LR, LGBM, WoE)	78.9%
	WoE	74.5%
	LR	77.0%
	LGBM	81.2%
	LR (PGA only)	77.2%
USGS Models	Godt et al. (2008)	69.5%
	Nowicki Jessee et al. (2018)	72.2%
	Nowicki et al. (2014)	72.1%

We can also compare model predictive power by estimating the number of expected landslides and comparing with observations. We have reclassified our models to provide an estimate for

spatial frequency of landslides. This estimate is based on the overall average spatial density of landslides from all earthquakes used in our models, as described earlier.

Figure A-10 shows the ensemble model's estimated landslide frequency across Haiti, along with the mapped landslides from Harp et al. (2016). When we sum these values across the total map area for Haiti, we get an estimated number of landslides ranging from a low value of 2,388 for the LGBM model to a high value of 5,012 for the LR model. The WoE model produces an estimate of 2,840 landslides, so that the average estimate from the three BGC models is 3,560 landslides. This estimate is much lower than the total number of landslides mapped by Hart et al. (2016), 23,568, and likely reflects the general variability in landslide density between different events around the globe. Some of this difference could be explained by relative soil moisture, which is not considered in the model and may have been elevated at the time of the earthquake.

Comparison between BGC and USGS models for the 2010 Haiti earthquake suggests that our models have better predictive power for that event, and they produce an expected number of landslides lower than, but in the same order of magnitude as, observations.

A.3.5. M7.8 Gorkha, Nepal Earthquake of 2015

The Haiti earthquake discussed previously was included in the data used to develop the model, and we therefore expected the model to give reasonable results. The next test was to apply the model to a different event, previously unseen by the model. We chose the M7.8 Gorkha event given its proximity to the Kingdom of Bhutan, similarity in terrain characteristics along the Himalaya, and similarity in magnitude to the M7 and M8 scenarios provided by Geozards International (GHI) for study.

Figure A-11 provides RoC curves for the full range of models considered, and their AUC values are listed in Table A-10. The estimated numbers of landslides from the various BGC models from approximately equal to the number in the most complete inventory of Roback et al. (2017) to approximately 2.5 times the number of mapped landslides. We consider this to be excellent performance for a global model, and therefore expect the BGC models to provide a reasonable basis for nation-scale predictions for the Kingdom of Bhutan. Among the full models (i.e., models that do not exclude PGV), the WoE prediction is closest to actual observations, and therefore may be most reliable when full Shakemap products are available. For the PGA-only models, which we will apply to the M7 and M8 scenario earthquakes, all three models (i.e., WoE, LR and the ensemble combination of the two) are equivalent to each other.

The BGC models include four that consider all potential seismic inputs and three that exclude PGV, for use with the PGA Shakemaps for Bhutan M7 and M8 scenarios. Ensemble models are also included, based on equal contribution from two models that exclude PGV (i.e., WoE and LR and three full models (i.e., WoE, LR and LGBM).

Unlike the results for Haiti, in this case the LGBM model is the worst performing BGC model, and WoE has the best predictive power. Given this variability in performance among the various models for the two different events, there may be value in considering an ensemble predictive

model for all future predictions. Performance of the BGC models is markedly better than that of the USGS models, with our best model having AUC ~ 10% better than the preferred USGS model of Nowicki Jessee et al. (2018).

As discussed previously for Haiti, we can again generate an estimate of the number of expected landslides. Estimates for each BGC model are provided in Table A-11. We have three different landslide inventories available for this event. Gnyawali et al. (2016) produced an inventory of 17,532 landslide points. Zhang et al. (2016) mapped 2,645 landslide polygons and Roback et al. (2017) mapped 24,915 landslide polygons, including source, transport and deposition zones. Roback et al. (2017) separately mapped the source zones for 24,795 landslides. Mapped landslides are shown over the BGC ensemble model prediction showing expected landslide density in Figure A-12.

The estimated numbers of landslides from the various BGC models range from approximately equal to the number in the most complete inventory of Roback et al. (2017) to approximately 2.5 times the number of mapped landslides. We consider this to be excellent performance for a global model, and therefore expect the BGC models to provide a reasonable basis for nation-scale predictions for the Kingdom of Bhutan. Among the full models (i.e., models that do not exclude PGV), the WoE prediction is closest to actual observations, and therefore may be most reliable when full Shakemap products are available. For the PGA-only models, which we will apply to the M7 and M8 scenario earthquakes, all three models (i.e., WoE, LR and the ensemble combination of the two) are equivalent to each other.

Table A-10. Model comparison for the 2015 Gorkha, Nepal M7.8 earthquake.

Model		RoC AUC
BGC Models (PGA only; excluding PGV)	Ensemble (PGA only)	84.4%
	WoE (PGA only)	85.4%
	LR (PGA only)	77.7%
BGC Models (full)	Ensemble (LR, LGBM, WoE)	83.9%
	WoE	85.4%
	LR	80.4%
	LGBM	79.9%
USGS Models	Godt et al. (2008)	69.9%
	Nowicki Jessee et al. (2018)	75.9%
	Nowicki et al. (2014)	78.1%

Table A-11. Expected numbers of landslides for the 2015 Gorkha, Nepal M7.8 earthquake.

Event	BGC Model	Expected landslides (total)
2015 M7.8 Gorkha, Nepal	Ensemble (PGA only)	26,221
	WoE (PGA only)	27,278
	LR (PGA only)	25,169
	Ensemble (LR, LGBM, WoE)	44,665
	WoE	29,032
	LR	62,359
	LGBM	42,609

A.4. MODEL APPLICATION TO THE KINGDOM OF BHUTAN

We first examine model performance against a 2009 M6.1 earthquake that occurred in eastern Bhutan. Complete Shakemap products are available from USGS for that event, so we first applied our full models to that earthquake. GHI provided PGA-only Shakemaps for two scenario earthquakes: M7 occurring along a fault along the western border of Bhutan, and M8 occurring along a fault along the full length of Bhutan's southern border. We applied our PGA-only models to those two scenario earthquake events. Figure A-13 shows the expected landslide density across Bhutan following the 2009 M6.1 event, and Figure A-14 shows the same result at a larger scale. Figure A-15 shows the result in comparison with the model prediction and mapped landslides for the 2015 Gorkha earthquake. Qualitatively, the model results suggest very few, if any, landslides in Bhutan following the 2009 event.

Figure A-16 shows PGA-only ensemble model results for the M7 Bhutan scenario earthquake, followed by a comparison with model predictions for the Gorkha earthquake in Figure A-17. Figures A-18 and A-19 show similar PGA-only ensemble model predictions and comparisons for the M8 Bhutan scenario event. Qualitatively, the M7 event is expected to produce far fewer landslides than the 2015 Gorkha earthquake, and they will be concentrated near the western border, close to the affected fault. The M8 scenario, by contrast, shows high expected landslide density across the country, with landslides expected to be more common in the southern half of the country.

As with the Haiti and Nepal earthquakes discussed previously, we can estimate the numbers of expected landslides associated with each considered earthquake event. In Table A-12 below, we summarize estimates for landslides in Bhutan associated with the three different earthquake scenarios under consideration, for each considered model. We distinguish between the total numbers of landslides expected across the whole Kingdom of Bhutan and those to be found within 200 m (i.e., 400 m wide corridor) along any road or any national highway.

As discussed in the previous subsection, we expect the full WoE model to give the best prediction, and it suggests one landslide along a 400 m corridor along national highways, or 18 landslides in the whole country. We understand from discussion with GHI and other project partners in a

progress meeting in October 2021 that no landslides were documented following that earthquake. It is therefore possible that our predictions err on the conservative side. It may also be possible that some landslides occurred, but were not observed or reported, given their distance from well-travelled roads.

Table A-12. Expected landslides for Bhutan earthquake scenario events.

Event	Model	Estimated Number of Landslides		
		Whole Bhutan	All roads (within 200 m)	National Highways (within 200 m)
2009 M6.1	Ensemble	263	26	6
	WoE	18	5	1
	LGBM	222	29	6
	LR	548	44	11
M7 Scenario	Ensemble (PGA only)	2196	144	38
	LR (PGA only)	3649	200	56
	WoE (PGA only)	754	88	20
M8 Scenario	Ensemble (PGA only)	38334	3998	877
	LR (PGA only)	35873	2716	604
	WoE (PGA only)	40885	5292	1150

Landslide predictions for the whole of Bhutan for the M8 scenario earthquake range between 35,873 and 40,885, somewhat higher than the PGA-only model predictions for the M7.8 Gorkha event as listed in Table A-11. The ensemble forecast for Bhutan is 38,333 landslides as compared with the 26,221 predicted for the Gorkha event. We may therefore expect that a M8 earthquake occurring along the southern border would likely produce widespread landslides, being potentially more widespread than those following the 2015 event in Nepal. By contrast, the M7 scenario is expected to produce an order of magnitude fewer landslides, with an ensemble model forecast of 2,196 landslides, of which 38 are expected along national highway corridors.

FIGURES

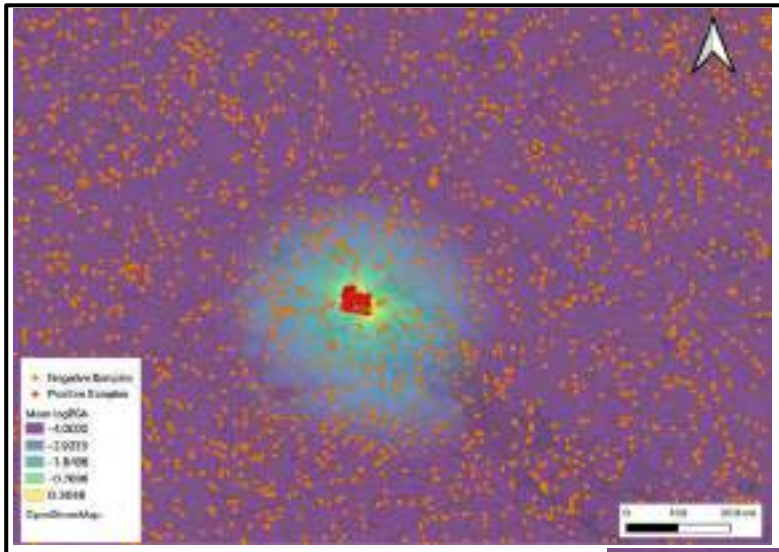

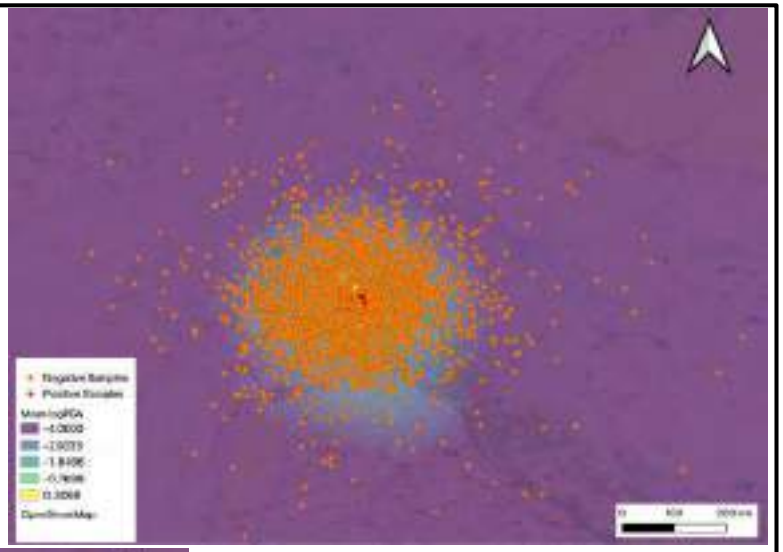

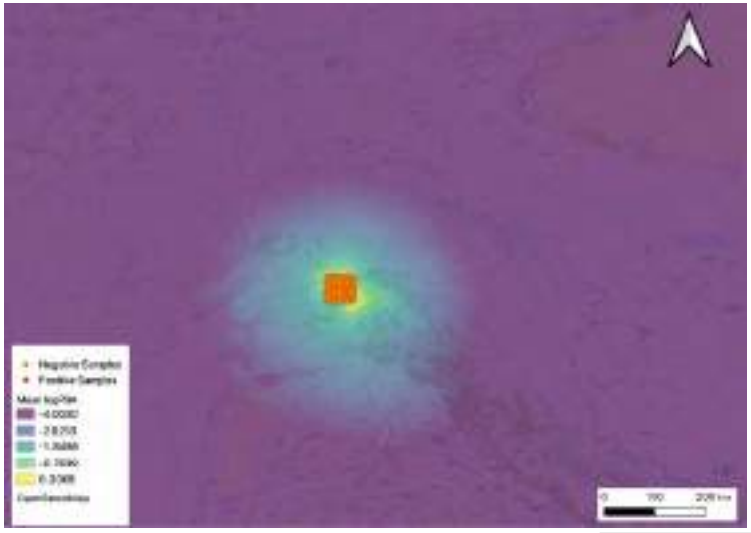

NOTES:

1. This Figure should be read in conjunction with BGC's report titled "Co-seismic landslide susceptibility map for the Kingdom of Bhutan," and dated May 2022.
2. Random across shakemap (top left), random across shakemap inverse distance weighted to center of landslide inventory (top right), random across extent of landslide inventory (bottom).

PREPARED BY:	FIGURE TITLE		
RS	Negative Sampling Schemes		
CHECKED BY:	CLIENT:		
KH	Royal Government of Bhutan and GeoHazards International		
APPROVED BY:	SCALE:	PROJECT NO:	FIGURE NO:
PQ	As shown	BGC21006	A-1

0 5 10 mm in ANSI A sized paper

BGC ENGINEERING INC.

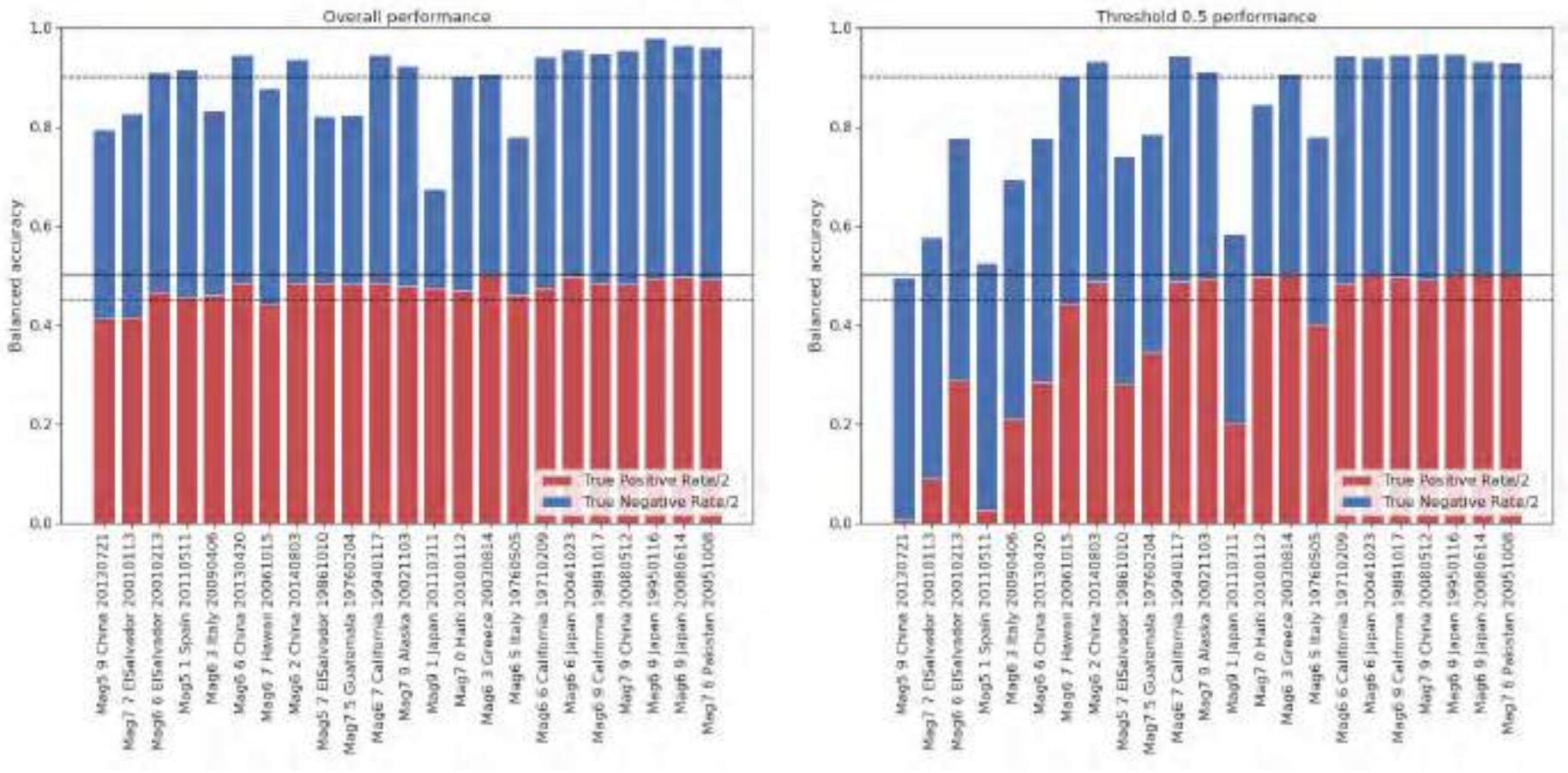

NOTES:

1. This Figure should be read in conjunction with BGC's report titled "Co-seismic landslide susceptibility map for the Kingdom of Bhutan," and dated May 2022.
2. Balanced accuracy metric for model LGBM model 773149 at best decision threshold (left) and a decision threshold of 0.5 (right). The events are sorted by ascending median logPGA across the landslide samples for each event. The solid black line represents a true positive rate of 100%. The top dashed black line represents a balanced accuracy of 90% and the bottom dashed black line represents a true positive rate of 90%.

PREPARED BY:	FIGURE TITLE		
RS	Balanced Accuracy Metrics – LGBM model		
CHECKED BY:	CLIENT:		
KH	Royal Government of Bhutan and GeoHazards International		
APPROVED BY:	SCALE:	PROJECT NO:	FIGURE NO:
PQ	As shown	BGC21006	A-2

0 5 10 mm in ANSI A sized paper

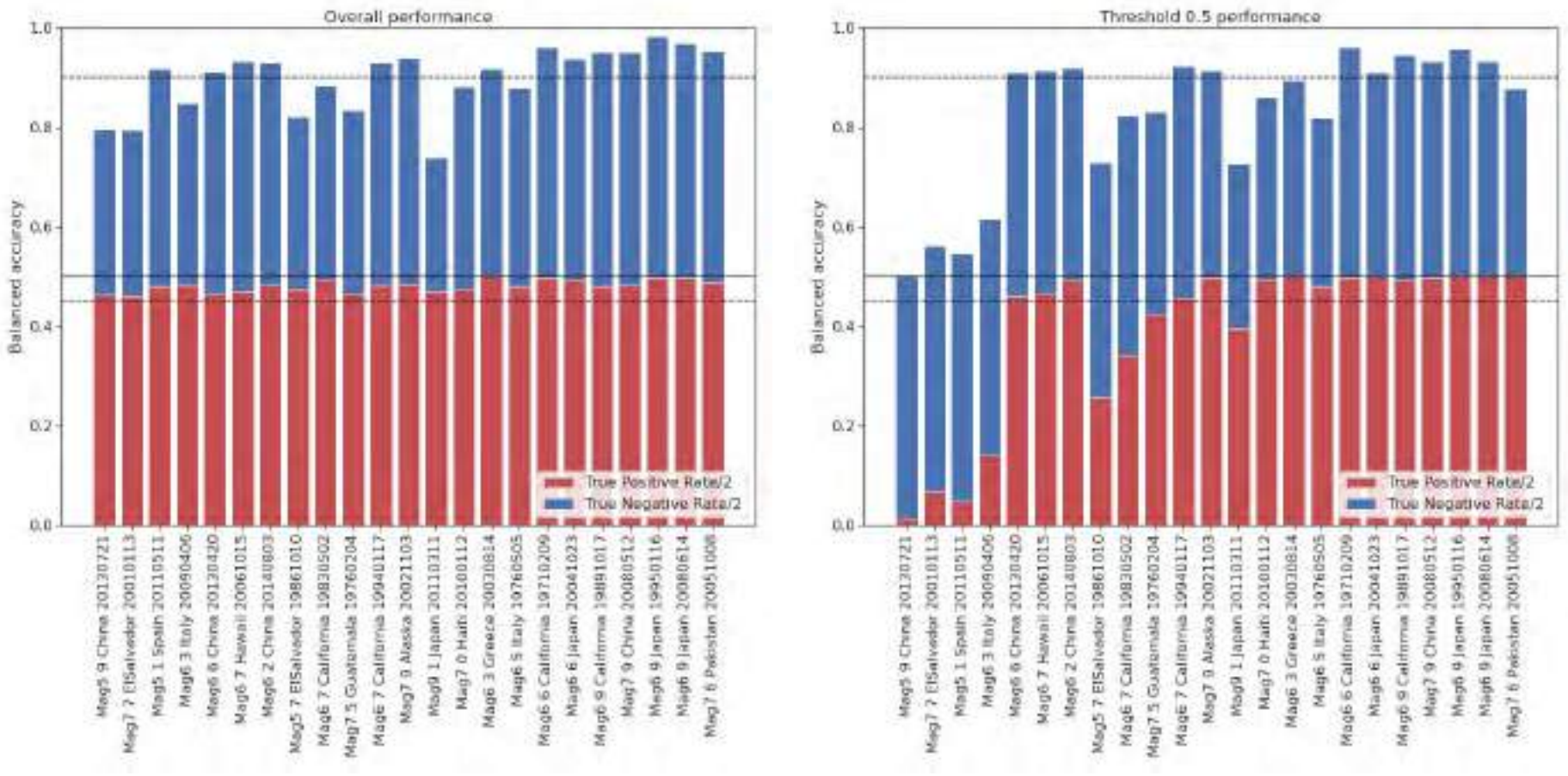

NOTES:

1. This Figure should be read in conjunction with BGC's report titled "Co-seismic landslide susceptibility map for the Kingdom of Bhutan," and dated May 2022.
2. Balanced accuracy metric for model LGBM model 773149 at best decision threshold (left) and a decision threshold of 0.5 (right). The events are sorted by ascending median logPGA across the landslide samples for each event. The solid black line represents a true positive rate of 100%. The top dashed black line represents a balanced accuracy of 90% and the bottom dashed black line represents a true positive rate of 90%.

PREPARED BY:	FIGURE TITLE		
RS	Balanced Accuracy Metrics – LR model		
CHECKED BY:	CLIENT:		
KH	Royal Government of Bhutan and GeoHazards International		
APPROVED BY:	SCALE:	PROJECT NO:	FIGURE NO:
PQ	As shown	BGC21006	A-2

0 5 10 mm in ANSI A sized paper

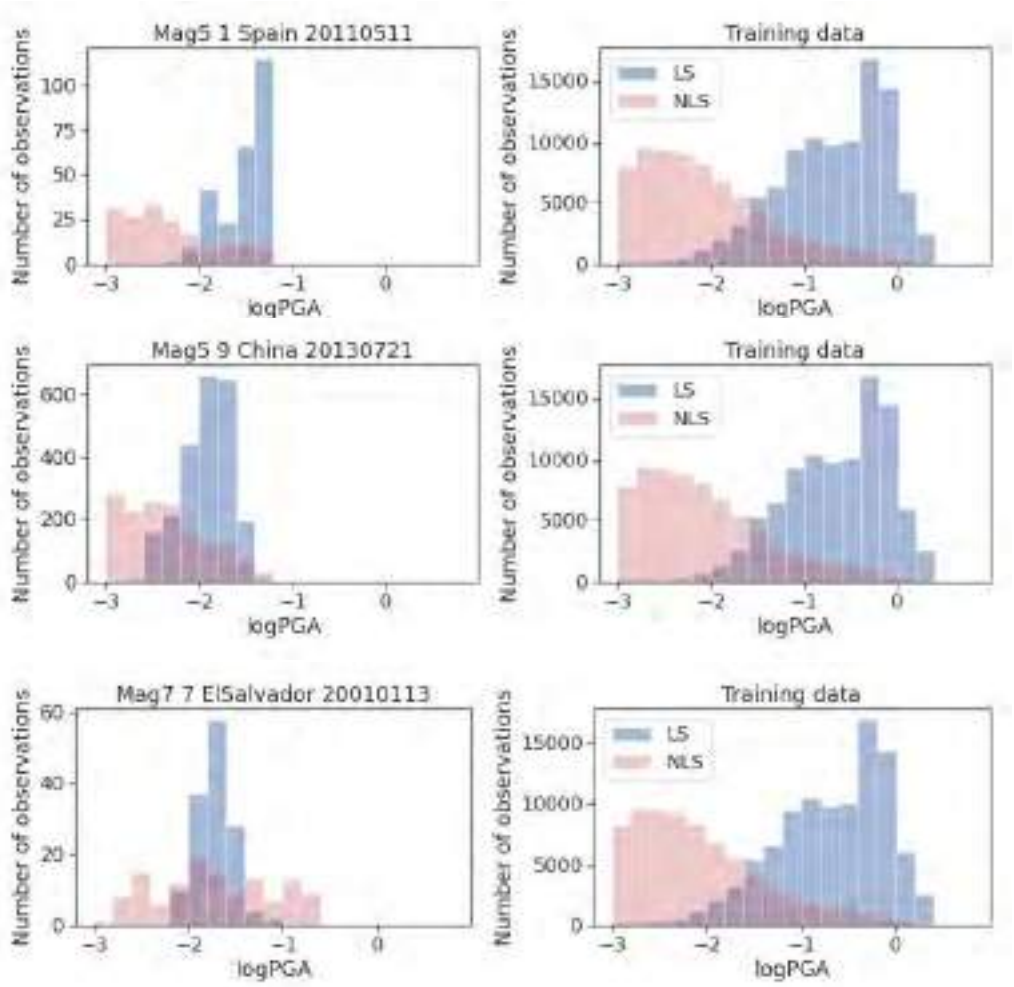

NOTES:

1. This Figure should be read in conjunction with BGC's report titled "Co-seismic landslide susceptibility map for the Kingdom of Bhutan," and dated May 2022.
2. A comparison of logPGA of Spain 5.1 2011, China 5.9 2013 and El Salvador 7.7 2001 against the training data for the fold each event was the validation event for.

PREPARED BY:	FIGURE TITLE		
RS	Landslide and non-landslide points for logPGA; various events		
CHECKED BY:	CLIENT:		
KH	Royal Government of Bhutan and GeoHazards International		
APPROVED BY:	SCALE:	PROJECT NO:	FIGURE NO:
PQ	As shown	BGC21006	A-4

0 5 10 mm in ANSI A sized paper

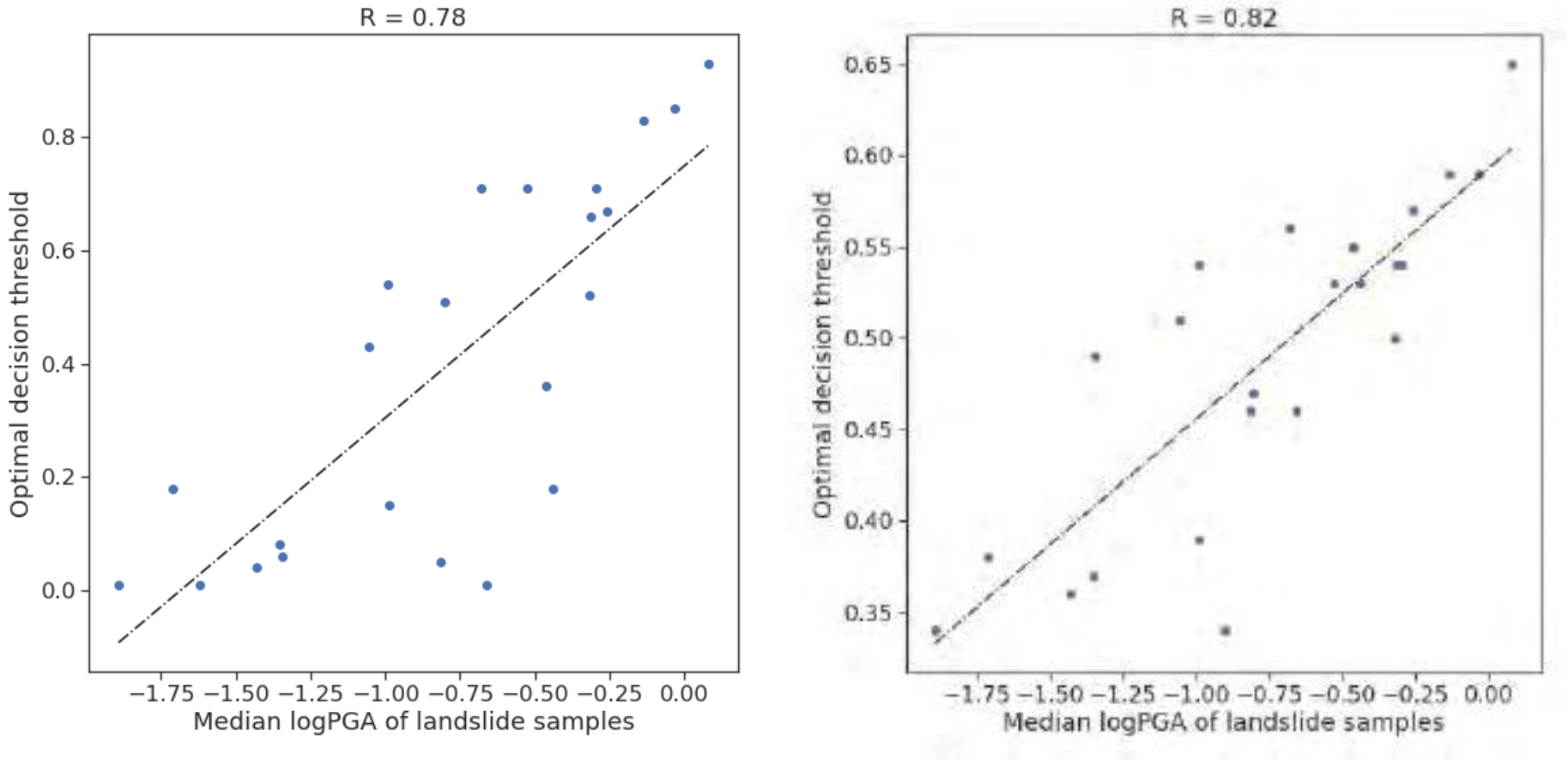

NOTES:

1. This Figure should be read in conjunction with BGC's report titled "Co-seismic landslide susceptibility map for the Kingdom of Bhutan," and dated May 2022.
2. Spearman correlation coefficient (R) between median logPGA of landslide samples and optimum decision threshold for LGBM model (left) and logistic regression model (right).

PREPARED BY: RS	FIGURE TITLE: Correlation coefficients at decision thresholds		
CHECKED BY: KH	CLIENT: Royal Government of Bhutan and GeoHazards International		
APPROVED BY: PQ	SCALE: As shown	PROJECT NO: BGC21006	FIGURE NO: A-5

0 5 10 mm in ANSI A sized paper

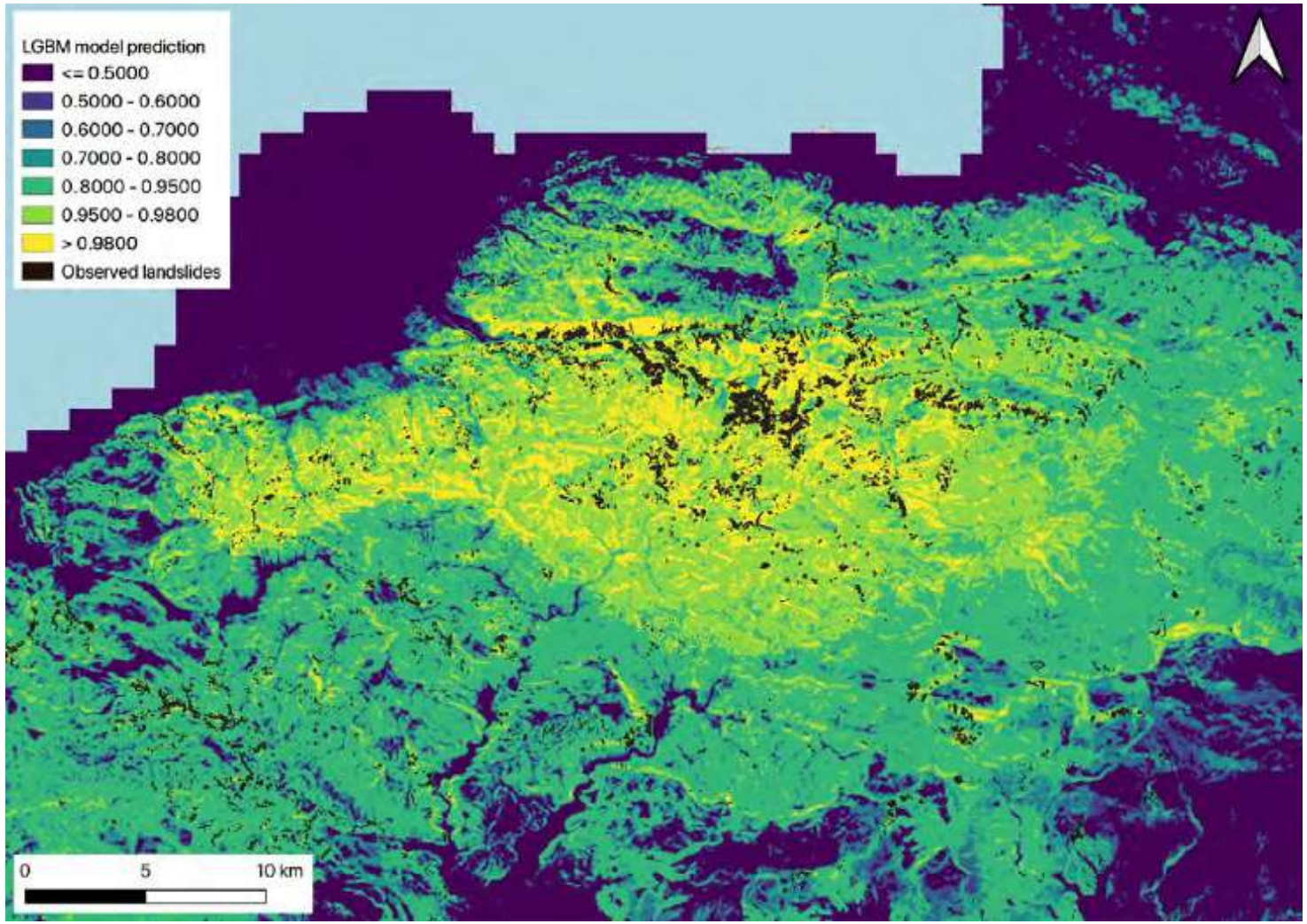

NOTES:

1. This Figure should be read in conjunction with BGC's report titled "Co-seismic landslide susceptibility map for the Kingdom of Bhutan," and dated May 2022.
2. Landslide score predicted by the LGBM model for the 2010-01-12 Magnitude 7.0 event in Haiti.

PREPARED BY: RS	FIGURE TITLE: Model result: LGBM model for 2010 Haiti M7.0 earthquake		
CHECKED BY: KH	CLIENT: Royal Government of Bhutan and GeoHazards International		
APPROVED BY: PQ	SCALE: As shown	PROJECT NO: BGC21006	FIGURE NO: A-6

0 5 10 mm in ANSI A sized paper

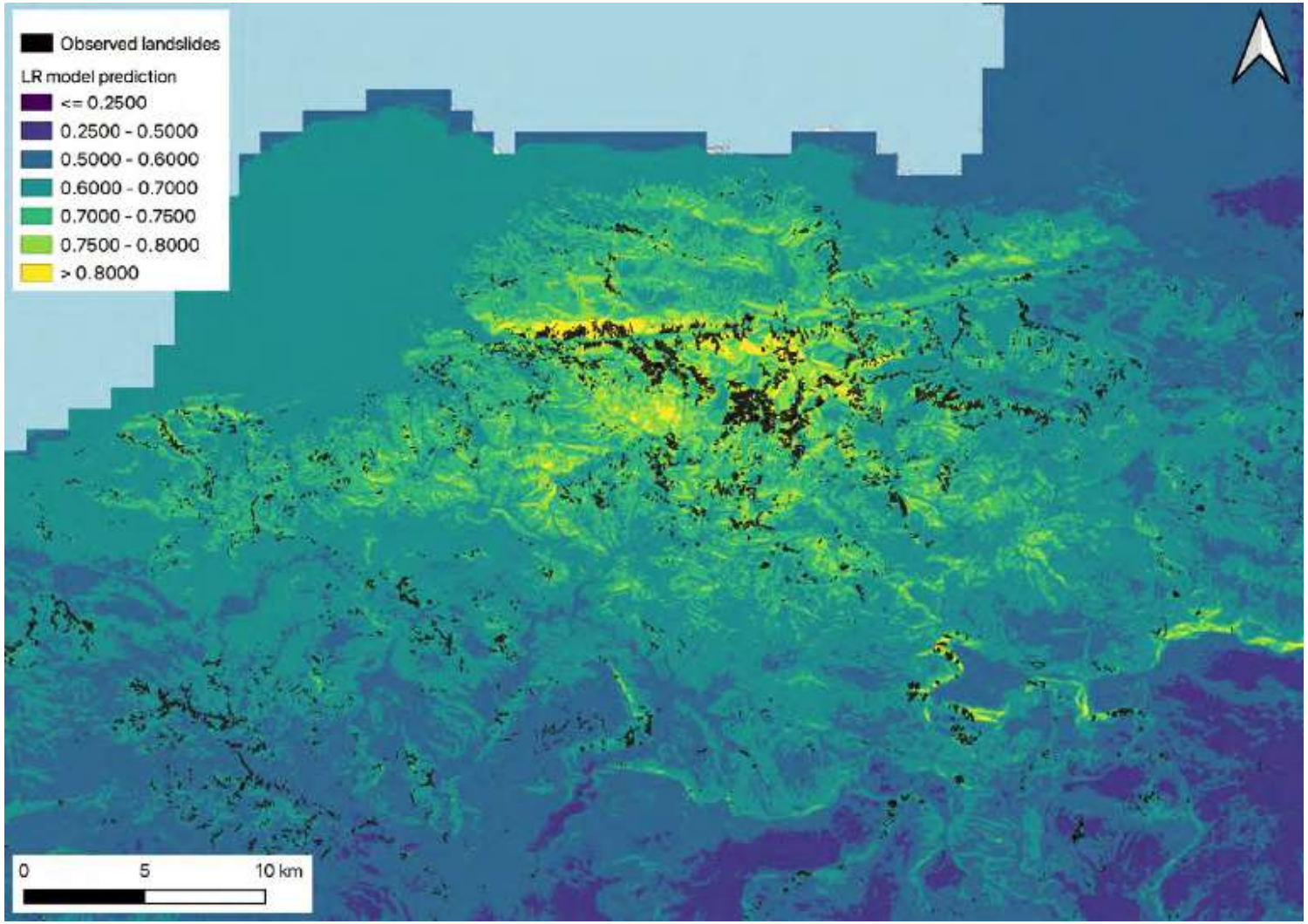

NOTES:

1. This Figure should be read in conjunction with BGC's report titled "Co-seismic landslide susceptibility map for the Kingdom of Bhutan," and dated May 2022.
2. Landslide score predicted by the LR model for the 2010-01-12 Magnitude 7.0 event in Haiti.

PREPARED BY: RS	FIGURE TITLE: Model result: LR model for 2010 Haiti M7.0 earthquake		
CHECKED BY: KH	CLIENT: Royal Government of Bhutan and GeoHazards International		
APPROVED BY: PQ	SCALE: As shown	PROJECT NO: BGC21006	FIGURE NO: A-7

0 5 10 mm in ANSI A sized paper

BGC ENGINEERING INC.

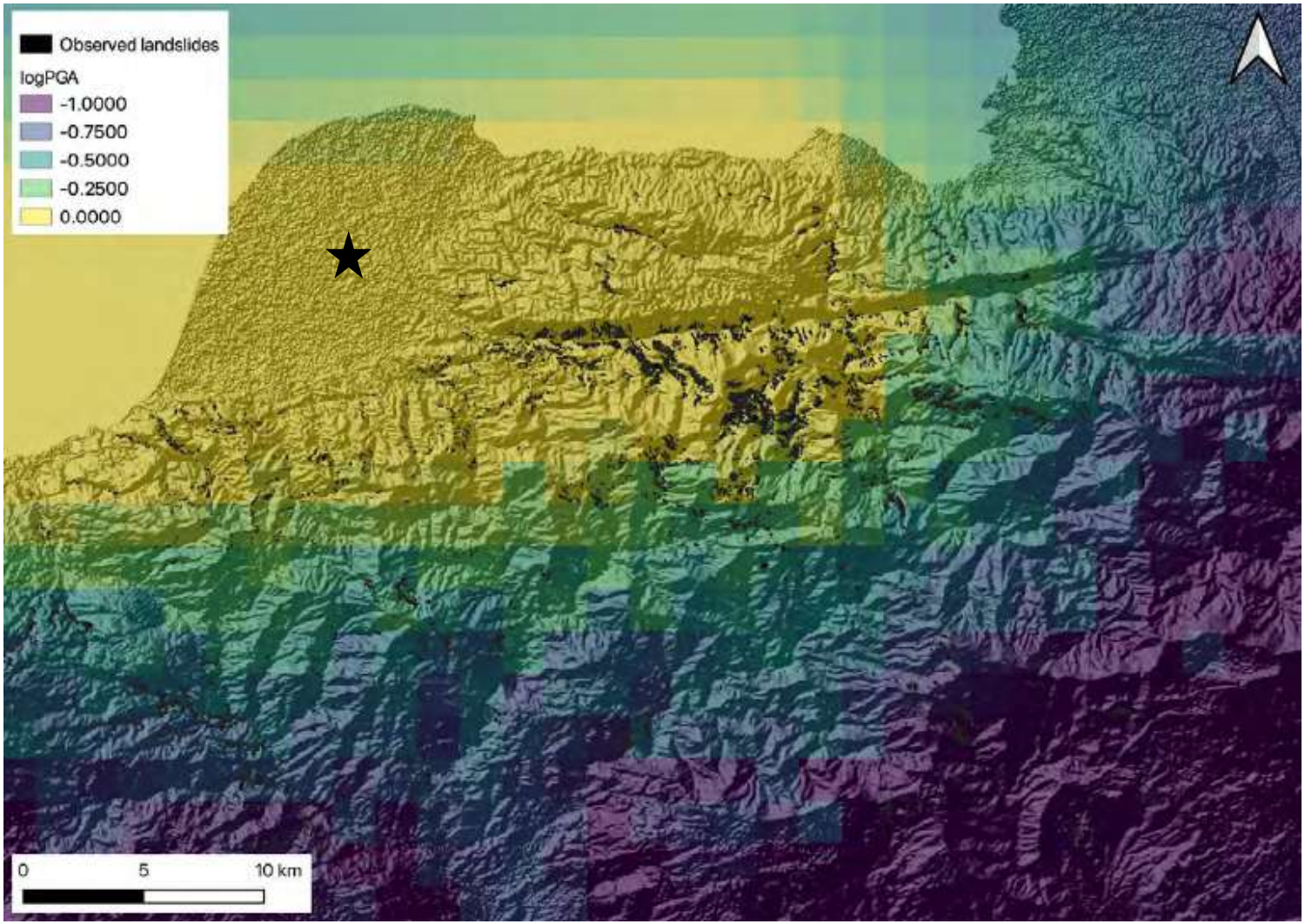

NOTES:

1. This Figure should be read in conjunction with BGC's report titled "Co-seismic landslide susceptibility map for the Kingdom of Bhutan," and dated May 2022.
2. The logPGA raster from the USGS shakemap overlaid on the SRTM DEM for the 2010-01-12 Magnitude 7.0 event in Haiti. The black star shows the relatively low-lying area with high logPGA values.

PREPARED BY:	FIGURE TITLE		
RS	logPGA for 2021 Haiti M7.0 earthquake		
CHECKED BY:	CLIENT:		
KH	Royal Government of Bhutan and GeoHazards International		
APPROVED BY:	SCALE:	PROJECT NO:	FIGURE NO:
PQ	As shown	BGC21006	A-8

0 5 10 mm in ANSI A sized paper

BGC ENGINEERING INC.

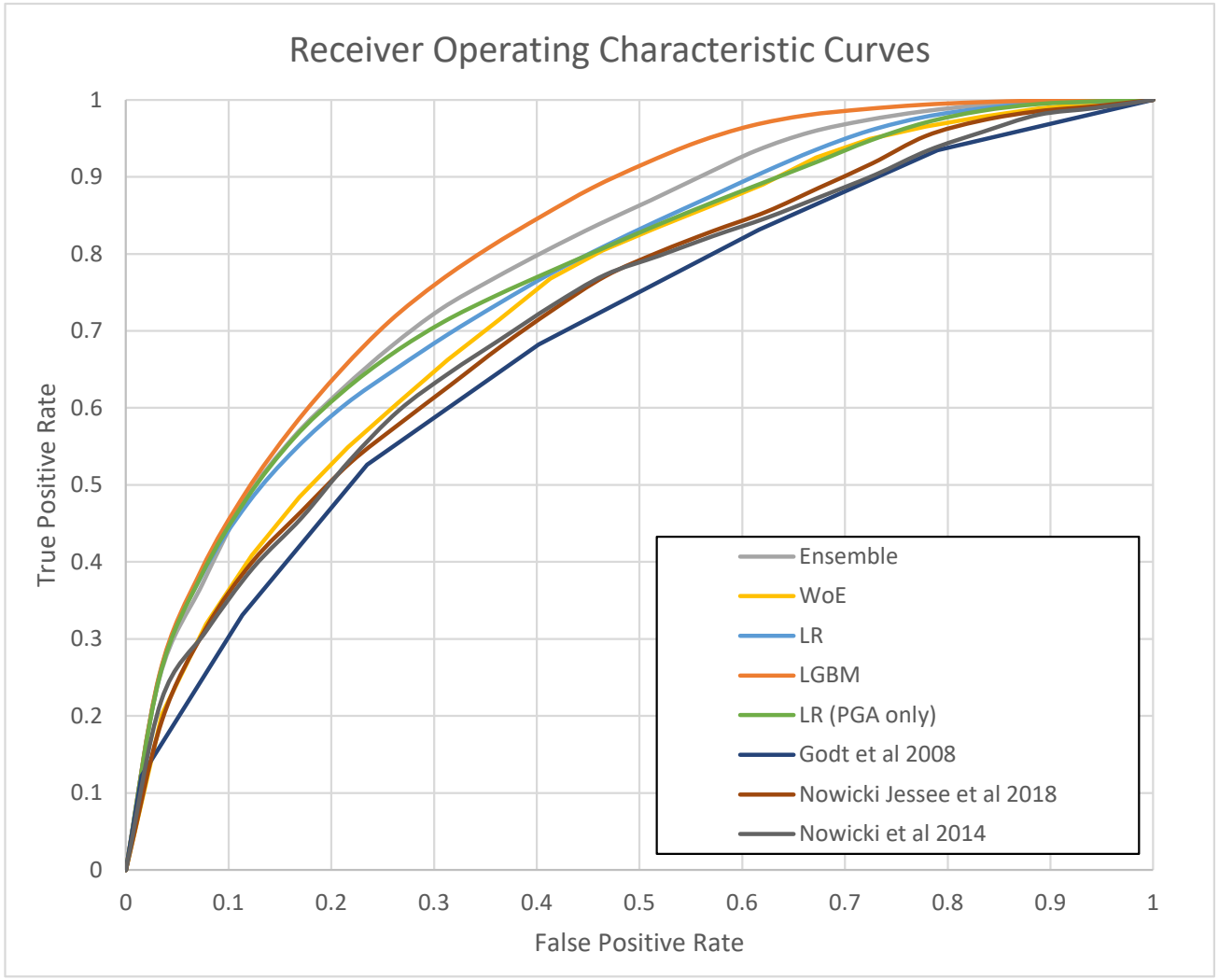

NOTES:

1. This Figure should be read in conjunction with BGC's report titled "Co-seismic landslide susceptibility map for the Kingdom of Bhutan," and dated May 2022.

PREPARED BY: PQ	FIGURE TITLE: Receiver operating characteristic curves – 2010 Haiti M7.0		
CHECKED BY: KH	CLIENT: Royal Government of Bhutan and GeoHazards International		
APPROVED BY: PQ	SCALE: As shown	PROJECT NO: BGC21006	FIGURE NO: A-9

0 5 10 mm in ANSI A sized paper

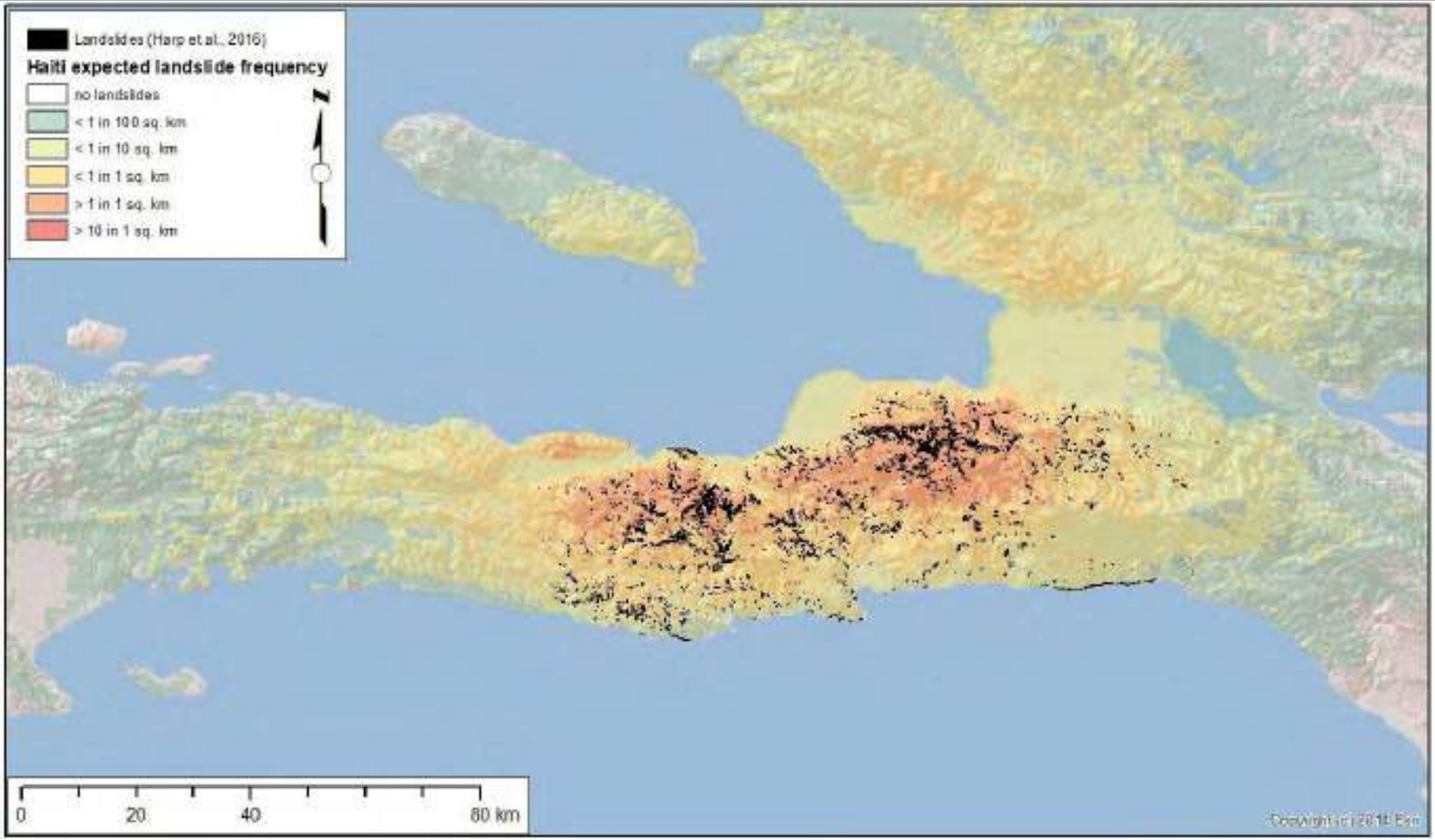

NOTES:

1. This Figure should be read in conjunction with BGC's report titled "Co-seismic landslide susceptibility map for the Kingdom of Bhutan," and dated May 2022.
2. Mapped landslides are taken from Harp et al. (2016).

PREPARED BY:	FIGURE TITLE		
PQ	Landslide prediction: Ensemble model, 2010 M7.0 Haiti		
CHECKED BY:	CLIENT:		
KH	Royal Government of Bhutan and GeoHazards International		
APPROVED BY:	SCALE:	PROJECT NO:	FIGURE NO:
PQ	As shown	BGC21006	A-10

0 5 10 mm in ANSI A sized paper

BGC ENGINEERING INC.

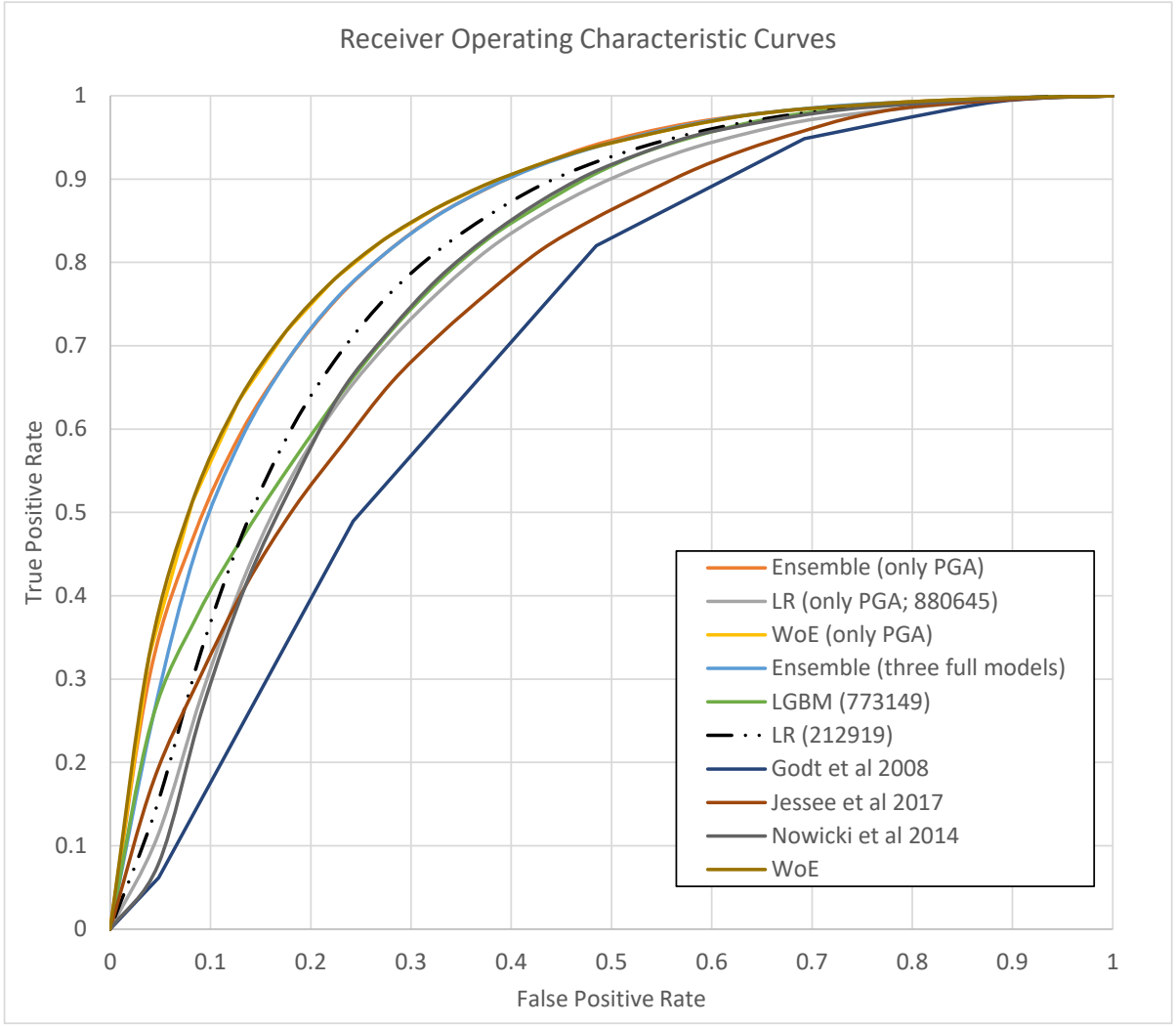

NOTES:

1. This Figure should be read in conjunction with BGC's report titled "Co-seismic landslide susceptibility map for the Kingdom of Bhutan," and dated May 2022.

PREPARED BY: PQ	FIGURE TITLE: Receiver operating characteristic curves – 2015 Nepal M7.8		
CHECKED BY: KH	CLIENT: Royal Government of Bhutan and GeoHazards International		
APPROVED BY: PQ	SCALE: As shown	PROJECT NO: BGC21006	FIGURE NO: A-11

0 5 10 mm in ANSI A sized paper

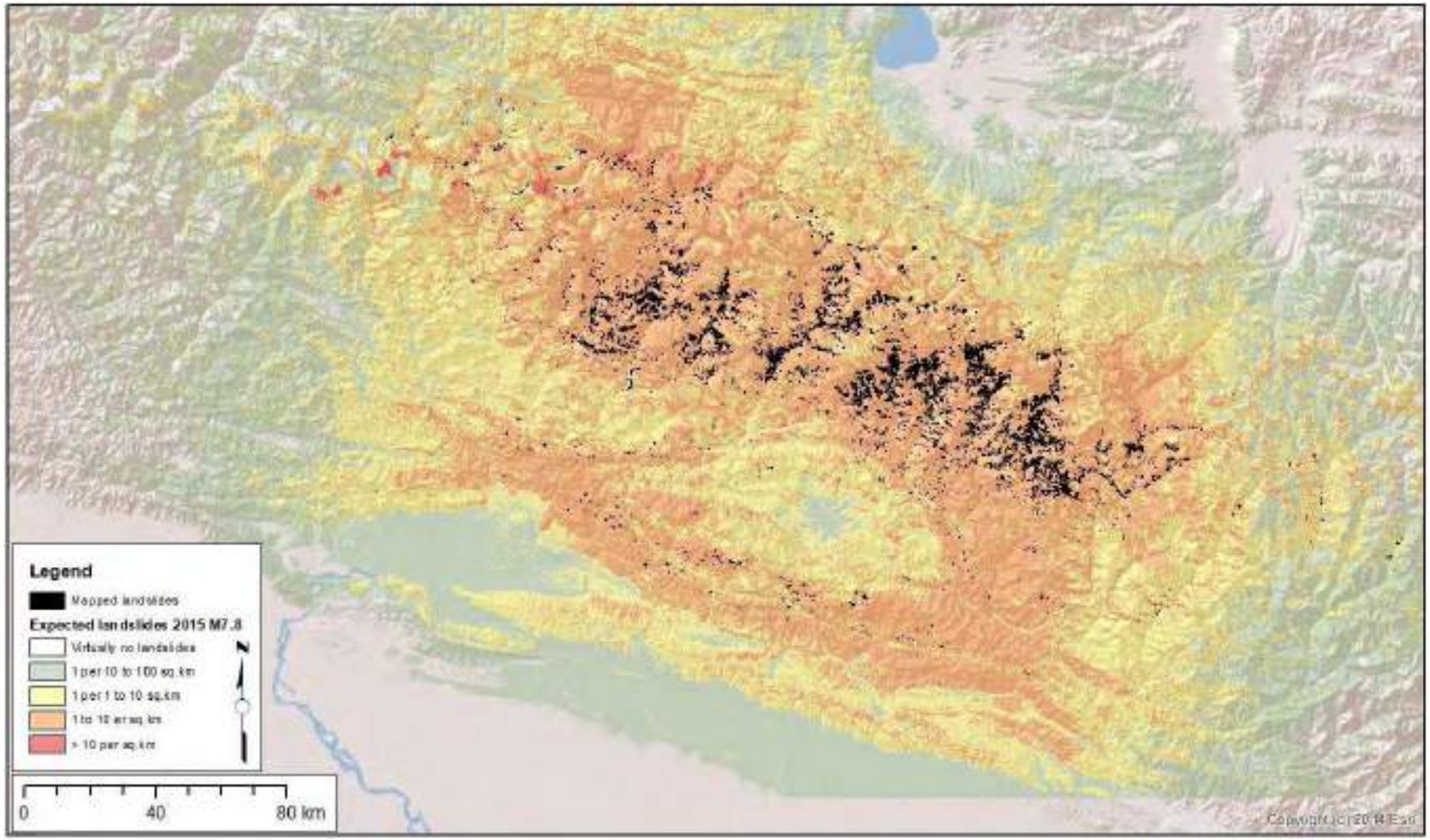

NOTES:

1. This Figure should be read in conjunction with BGC's report titled "Co-seismic landslide susceptibility map for the Kingdom of Bhutan," and dated May 2022.
2. Landslide data are taken from Gnyawali et al. (2016), Zhang et al. (2016) and Roback et al. (2017).

PREPARED BY:	FIGURE TITLE		
PQ	Landslide prediction: Ensemble model, 2015 M7.8 Gorkha		
CHECKED BY:	CLIENT:		
KH	Royal Government of Bhutan and GeoHazards International		
APPROVED BY:	SCALE:	PROJECT NO:	FIGURE NO:
PQ	As shown	BGC21006	A-12

0 5 10 mm in ANSI A sized paper

BGC ENGINEERING INC.

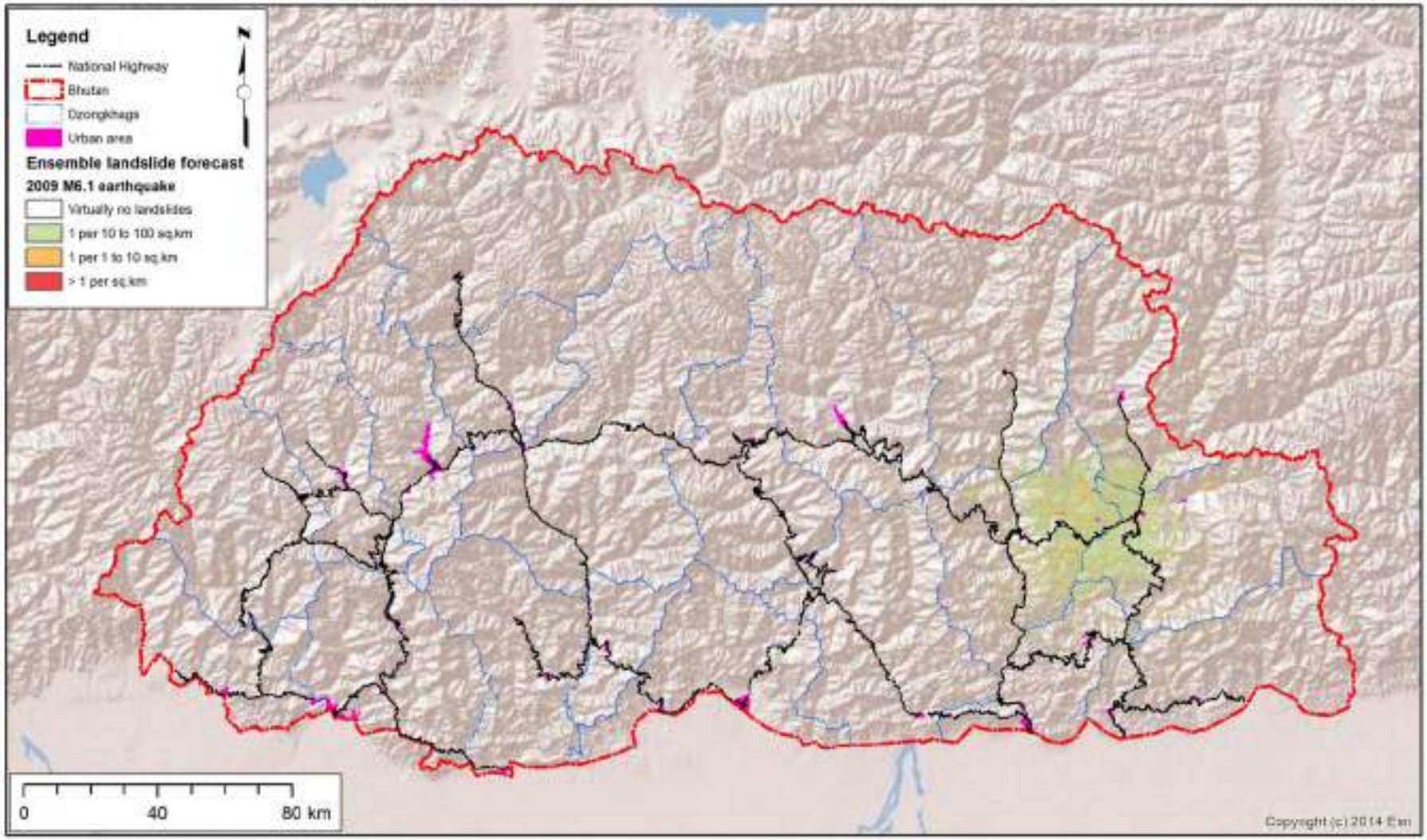

NOTES:

1. This Figure should be read in conjunction with BGC's report titled "Co-seismic landslide susceptibility map for the Kingdom of Bhutan," and dated May 2022.
2. Bhutan roads and urban areas provided by GeoHazards International.

PREPARED BY: PQ	FIGURE TITLE: Landslide prediction: Ensemble model, 2009 M6.1 Bhutan		
CHECKED BY: KH	CLIENT: Royal Government of Bhutan and GeoHazards International		
APPROVED BY: PQ	SCALE: As shown	PROJECT NO: BGC21006	FIGURE NO: A-13

0 5 10 mm in ANSI A sized paper

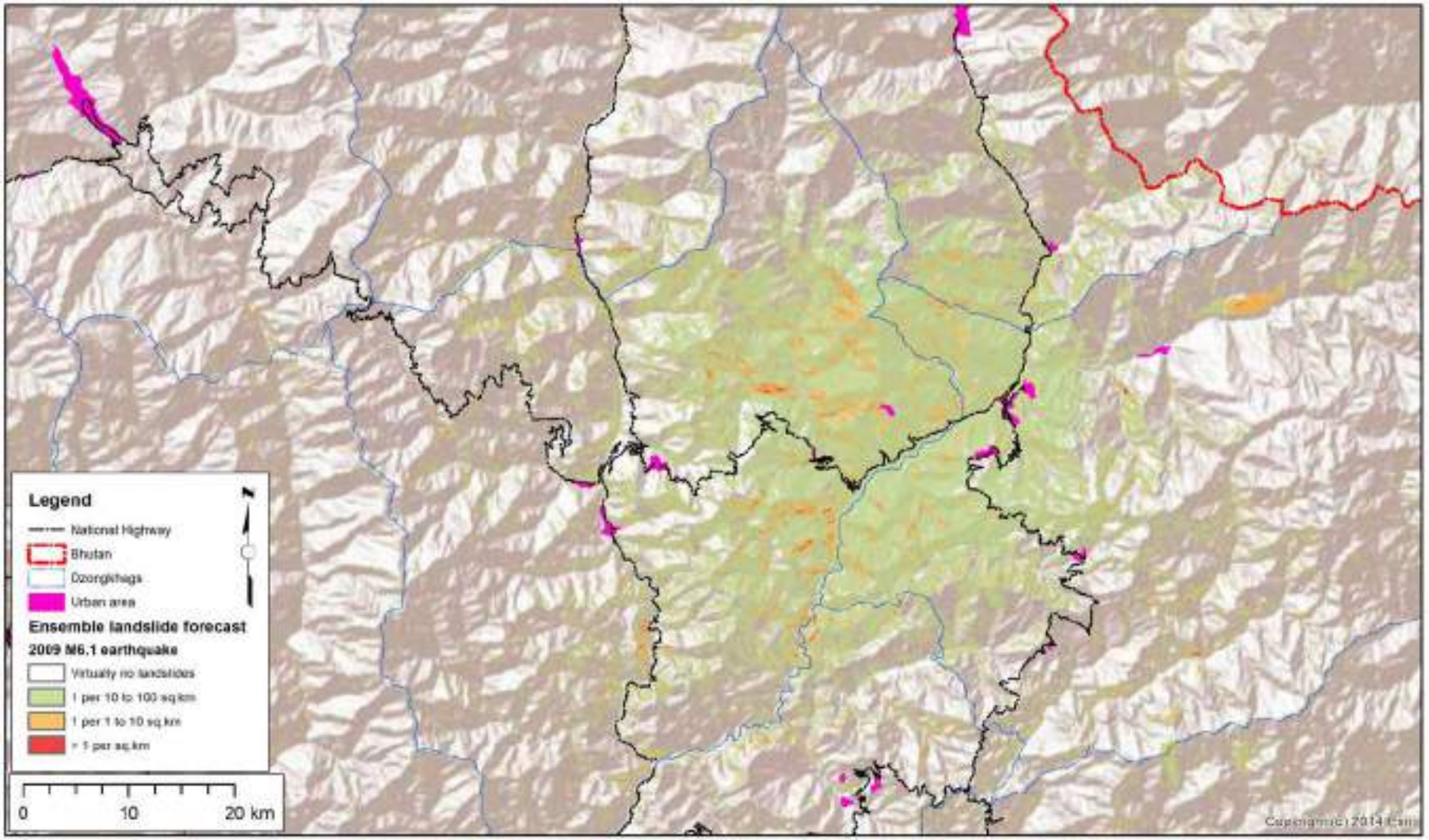

NOTES:

1. This Figure should be read in conjunction with BGC's report titled "Co-seismic landslide susceptibility map for the Kingdom of Bhutan," and dated May 2022.
2. Bhutan roads and urban areas provided by GeoHazards International.

PREPARED BY: PQ	FIGURE TITLE: Landslide prediction (zoom): Ensemble model, 2009 M6.1 Bhutan		
CHECKED BY: KH	CLIENT: Royal Government of Bhutan and GeoHazards International		
APPROVED BY: PQ	SCALE: As shown	PROJECT NO: BGC21006	FIGURE NO: A-14

0 5 10 mm in ANSI A sized paper

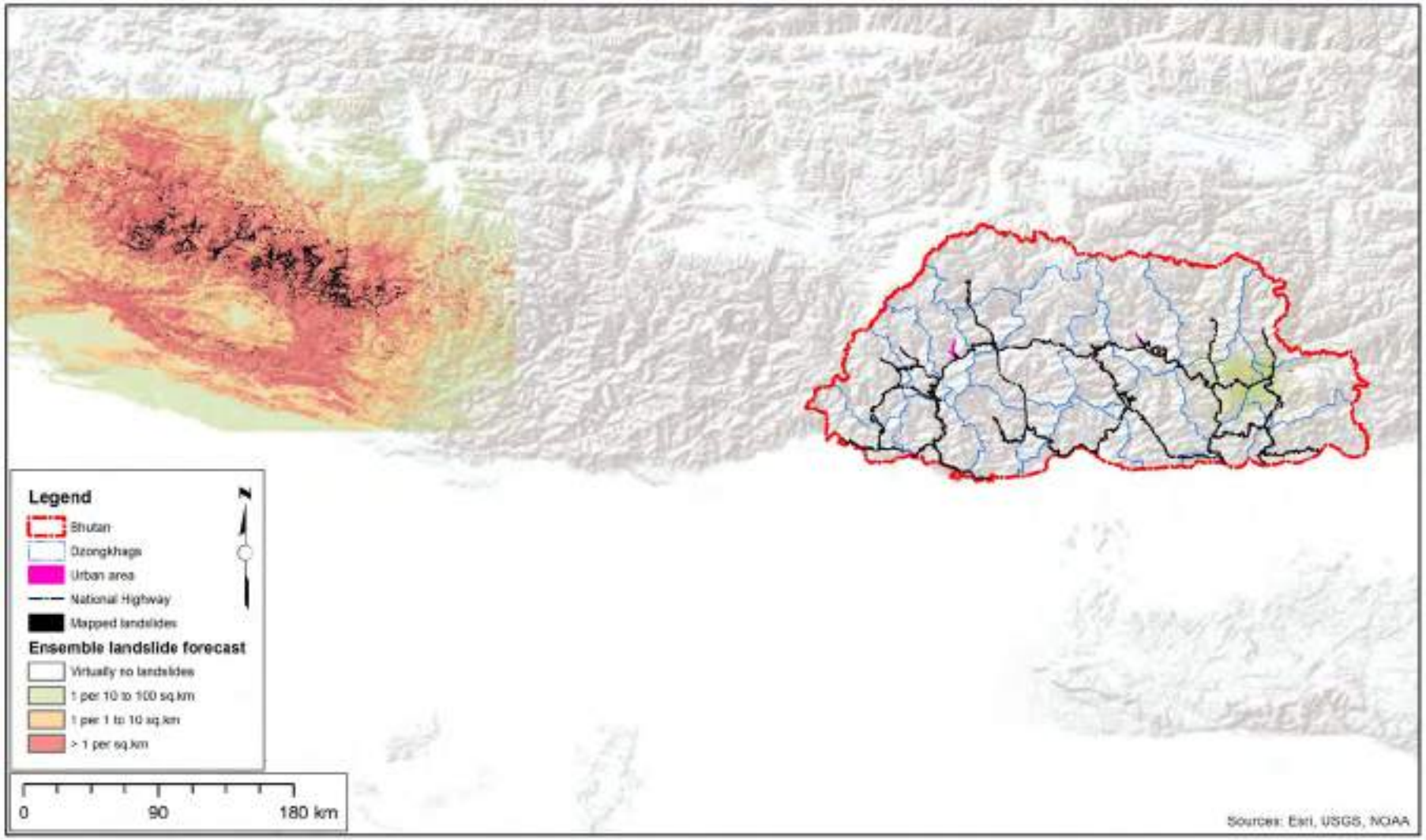

NOTES:

1. This Figure should be read in conjunction with BGC's report titled "Co-seismic landslide susceptibility map for the Kingdom of Bhutan," and dated May 2022.
2. Bhutan roads and urban areas provided by GeoHazards International.
3. Landslide data are taken from Gnyawali et al. (2016), Zhang et al. (2016) and Roback et al. (2017).

PREPARED BY:	FIGURE TITLE		
PQ	Comparison of predictions for Bhutan M6.1 and Gorkha M7.8		
CHECKED BY:	CLIENT:		
KH	Royal Government of Bhutan and GeoHazards International		
APPROVED BY:	SCALE:	PROJECT NO:	FIGURE NO:
PQ	As shown	BGC21006	A-15

0 5 10 mm in ANSI A sized paper

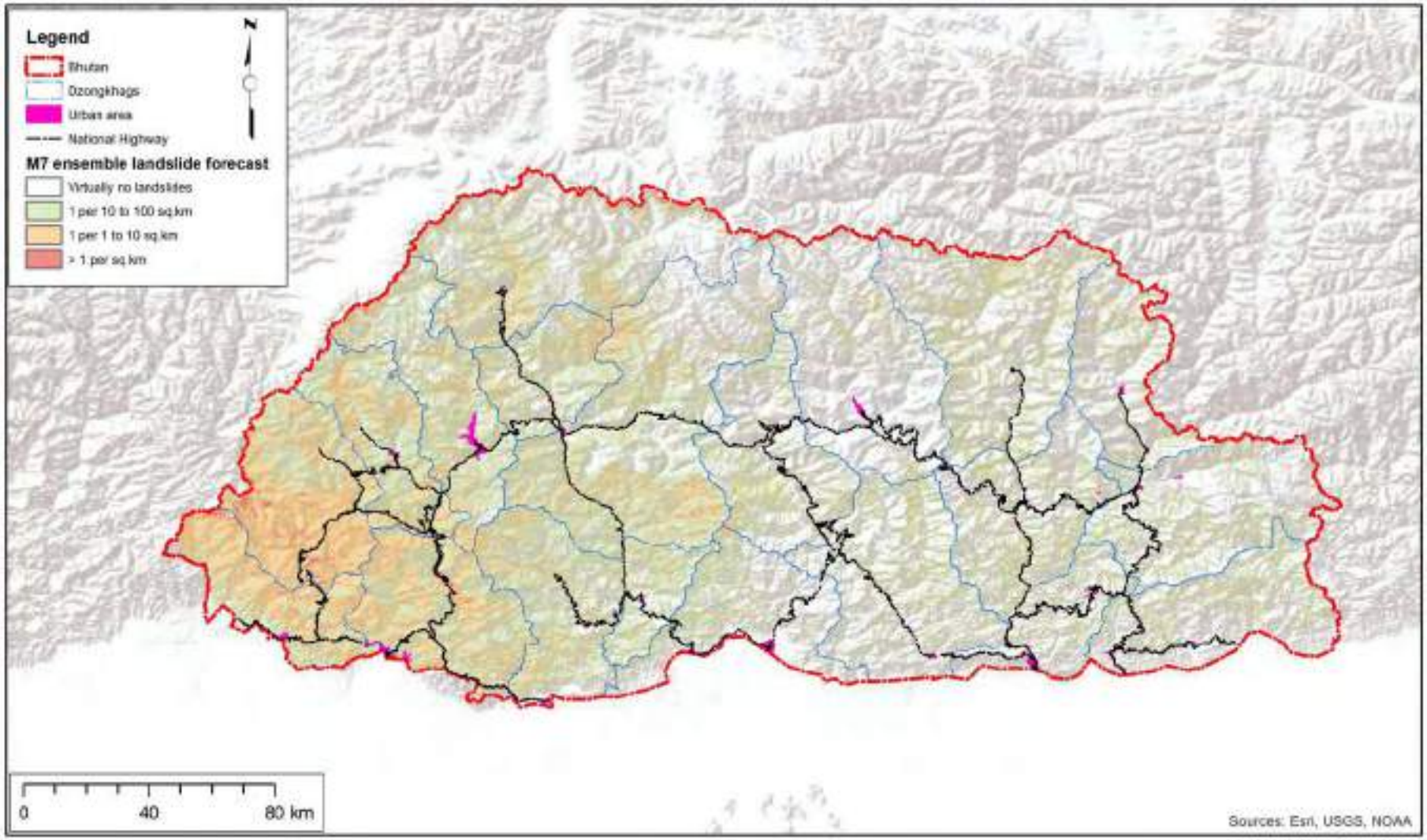

NOTES:

1. This Figure should be read in conjunction with BGC's report titled "Co-seismic landslide susceptibility map for the Kingdom of Bhutan," and dated May 2022.
2. Bhutan roads and urban areas provided by GeoHazards International.
3. M7 scenario shakemap with PGA provided by GeoHazards International.

PREPARED BY:	FIGURE TITLE		
PQ	Landslide prediction: Ensemble model, Bhutan M7 scenario		
CHECKED BY:	CLIENT:		
KH	Royal Government of Bhutan and GeoHazards International		
APPROVED BY:	SCALE:	PROJECT NO:	FIGURE NO:
PQ	As shown	BGC21006	A-16

0 5 10 mm in ANSI A sized paper

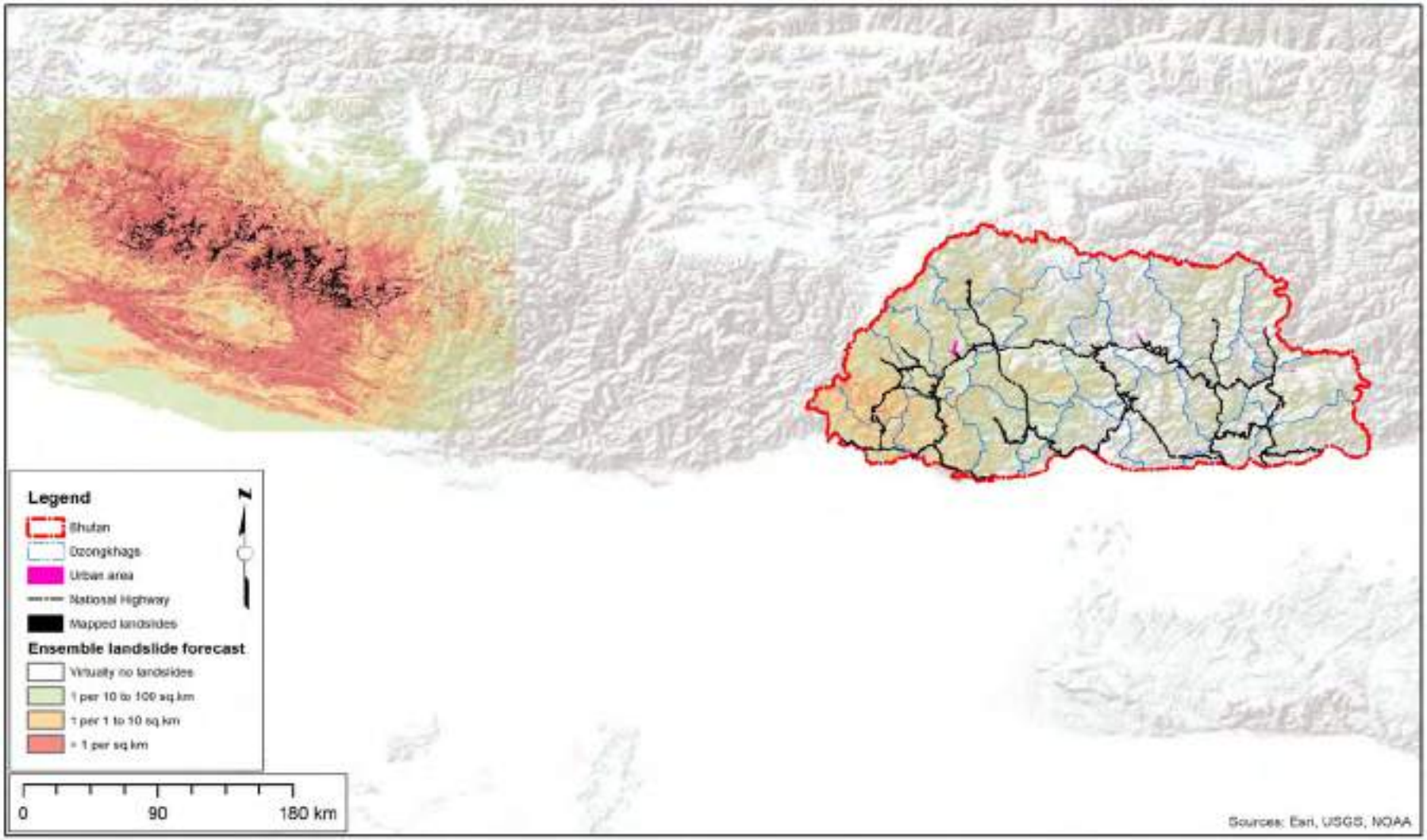

NOTES:

1. This Figure should be read in conjunction with BGC's report titled "Co-seismic landslide susceptibility map for the Kingdom of Bhutan," and dated May 2022.
2. Bhutan roads and urban areas provided by GeoHazards International.
3. M7 scenario shakemap with PGA provided by GeoHazards International.

PREPARED BY:	FIGURE TITLE		
PQ	Comparison of predictions for Bhutan M7 scenario and Gorkha M7.8		
CHECKED BY:	CLIENT:		
KH	Royal Government of Bhutan and GeoHazards International		
APPROVED BY:	SCALE:	PROJECT NO:	FIGURE NO:
PQ	As shown	BGC21006	A-17

0 5 10 mm in ANSI A sized paper

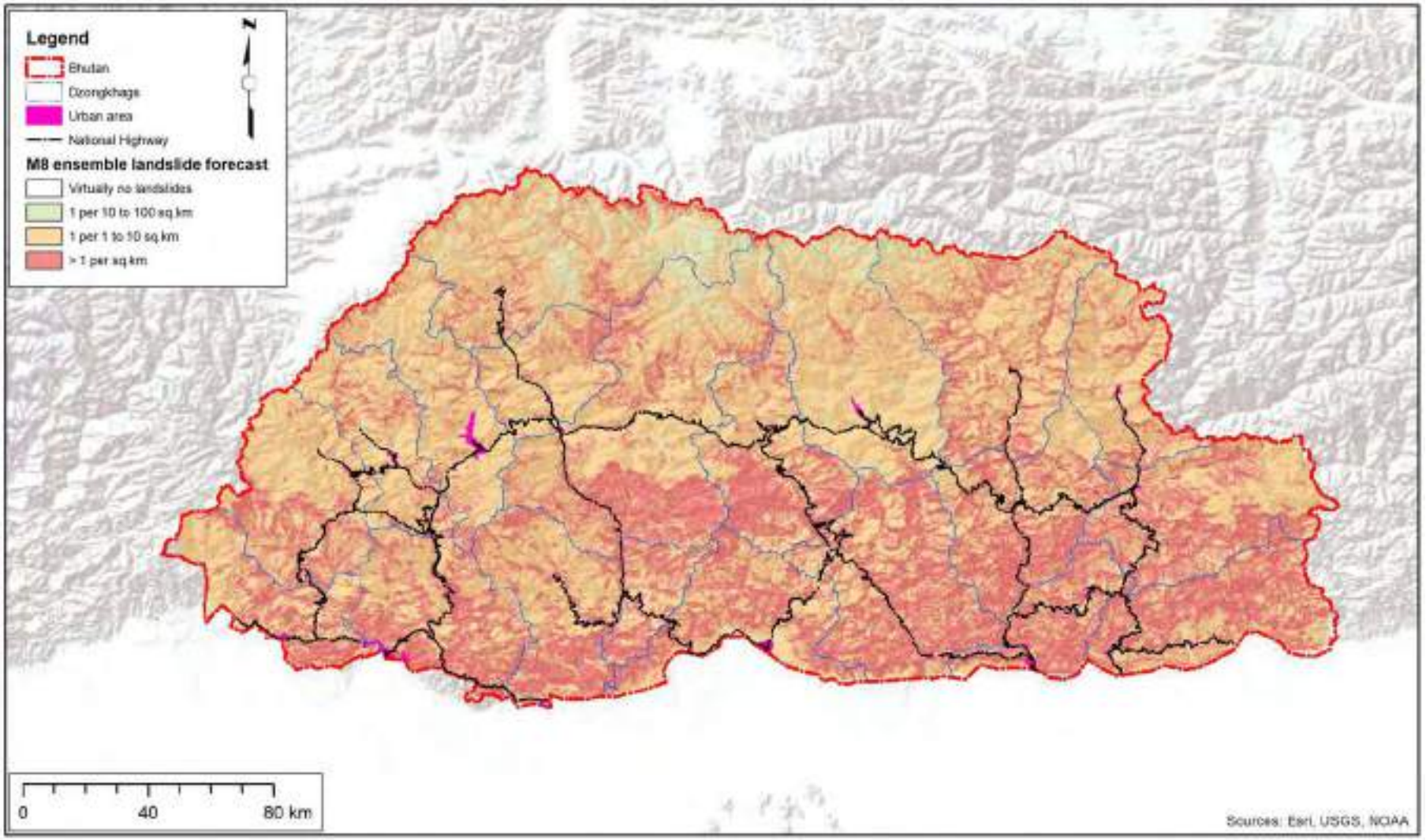

NOTES:

1. This Figure should be read in conjunction with BGC's report titled "Co-seismic landslide susceptibility map for the Kingdom of Bhutan," and dated May 2022.
2. Bhutan roads and urban areas provided by GeoHazards International.
3. M8 scenario shakemap with PGA provided by GeoHazards International.

PREPARED BY:	FIGURE TITLE		
PQ	Landslide prediction: Ensemble model, Bhutan M8 scenario		
CHECKED BY:	CLIENT:		
KH	Royal Government of Bhutan and GeoHazards International		
APPROVED BY:	SCALE:	PROJECT NO:	FIGURE NO:
PQ	As shown	BGC21006	A-18

0 5 10 mm in ANSI A sized paper

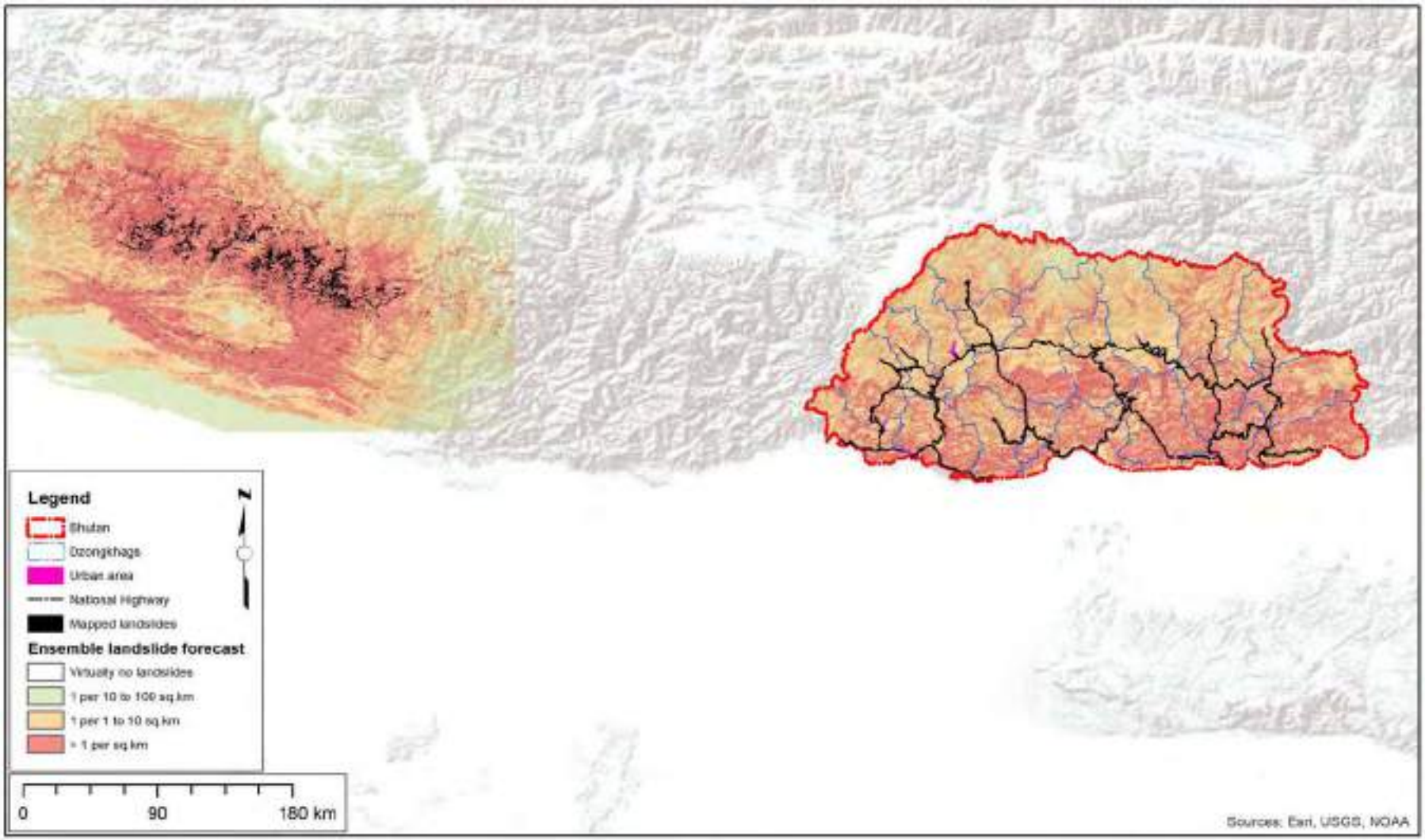

NOTES:

1. This Figure should be read in conjunction with BGC's report titled "Co-seismic landslide susceptibility map for the Kingdom of Bhutan," and dated May 2022.
2. Bhutan roads and urban areas provided by GeoHazards International.
3. M8 scenario shakemap with PGA provided by GeoHazards International.

PREPARED BY:	FIGURE TITLE		
PQ	Comparison of predictions for Bhutan M8 scenario and Gorkha M7.8		
CHECKED BY:	CLIENT:		
KH	Royal Government of Bhutan and GeoHazards International		
APPROVED BY:	SCALE:	PROJECT NO:	FIGURE NO:
PQ	As shown	BGC21006	A-19

0 5 10 mm in ANSI A sized paper

DRAWINGS

Coseismic Landslide Susceptibility Output for M7 Earthquake Scenario

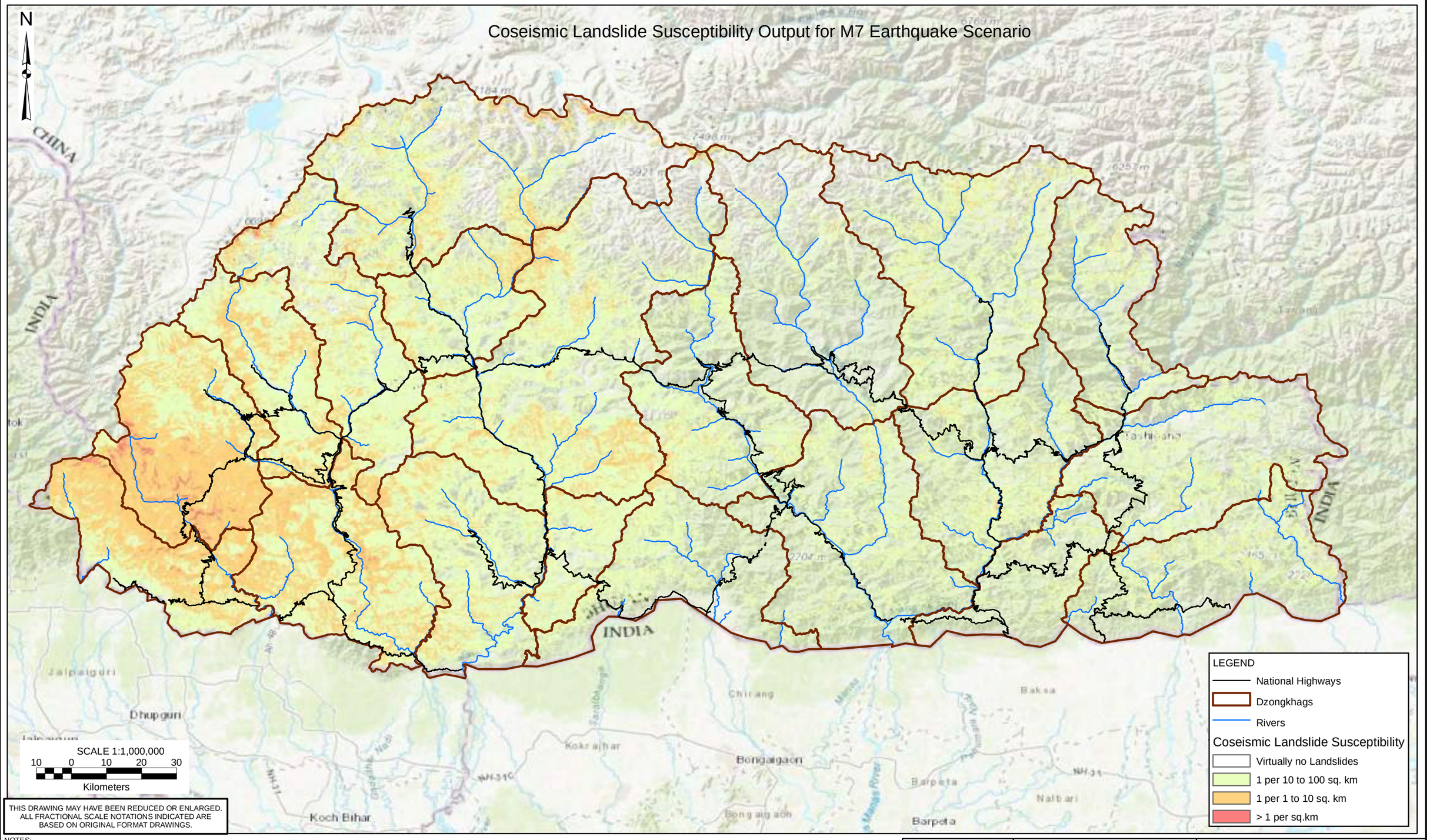

THIS DRAWING MAY HAVE BEEN REDUCED OR ENLARGED. ALL FRACTIONAL SCALE NOTATIONS INDICATED ARE BASED ON ORIGINAL FORMAT DRAWINGS.

NOTES:
1. ALL DIMENSIONS ARE IN METRES UNLESS OTHERWISE NOTED.
2. THIS DRAWING MUST BE READ IN CONJUNCTION WITH BGC'S REPORT TITLED "COSEISMIC LANDSLIDE SUSCEPTIBILITY MAP FOR THE KINGDOM OF BHUTAN", AND DATED MAY 2022.
3. BASE TOPOGRAPHIC DATA BASED ON SRTM DEM.
4. COORDINATE SYSTEM IS GCS WGS 1984. VERTICAL DATUM IS UNKNOWN.
5. UNLESS BGC AGREES OTHERWISE IN WRITING, THIS DRAWING SHALL NOT BE MODIFIED OR USED FOR ANY PURPOSE OTHER THAN THE PURPOSE FOR WHICH BGC GENERATED IT. BGC SHALL HAVE NO LIABILITY FOR ANY DAMAGES OR LOSS ARISING IN ANY WAY FROM ANY USE OR MODIFICATION OF THIS DOCUMENT NOT AUTHORIZED BY BGC. ANY USE OF OR RELIANCE UPON THIS DOCUMENT OR ITS CONTENT BY THIRD PARTIES SHALL BE AT SUCH THIRD PARTIES' SOLE RISK.

	1:1,000,000
DATE:	MAY 2022
DRAWN:	RDC
CHECKED:	PQ
APPROVED:	KH

BGC ENGINEERING INC.
AN APPLIED EARTH SCIENCES COMPANY

CLIENT: Geohazards International

Coseismic Landslide Susceptibility Mapping for the Kingdom of Bhutan

TITLE: Results for M7 Earthquake Scenario

PROJECT No.: BGC21006

DWG No: 001

C:\Users\rcarter\BGC Engineering Inc\BGC_Squared - GHI Bhutan\04_Reporting\03_Report\FINAL\m7.mxd

Coseismic Landslide Susceptibility Output for M8 Earthquake Scenario

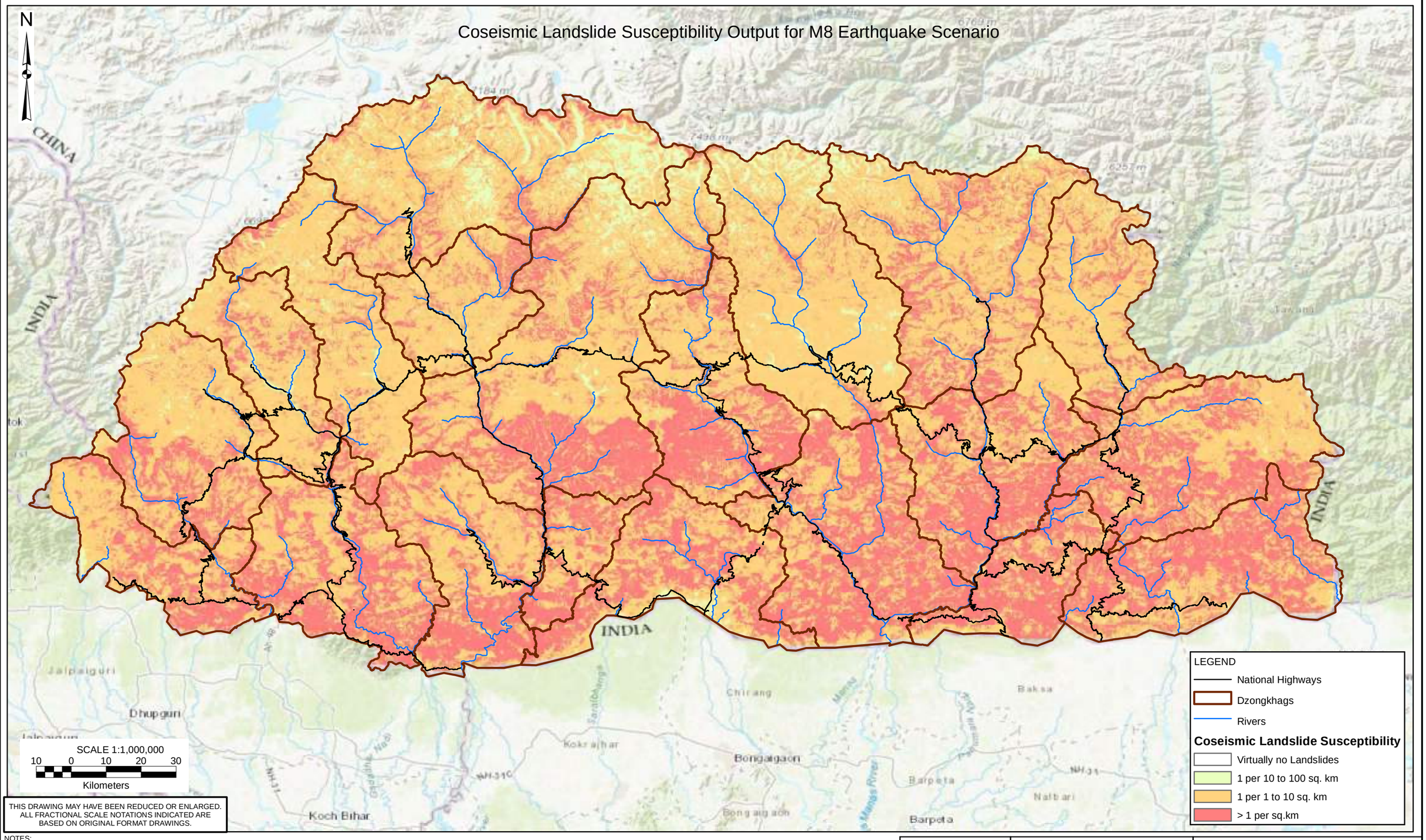

THIS DRAWING MAY HAVE BEEN REDUCED OR ENLARGED. ALL FRACTIONAL SCALE NOTATIONS INDICATED ARE BASED ON ORIGINAL FORMAT DRAWINGS.

NOTES:
1. ALL DIMENSIONS ARE IN METRES UNLESS OTHERWISE NOTED.
2. THIS DRAWING MUST BE READ IN CONJUNCTION WITH BGC'S REPORT TITLED "COSEISMIC LANDSLIDE SUSCEPTIBILITY MAP FOR THE KINGDOM OF BHUTAN", AND DATED MAY 2022.
3. BASE TOPOGRAPHIC DATA BASED ON SRTM DEM.
4. COORDINATE SYSTEM IS GCS WGS 1984. VERTICAL DATUM IS UNKNOWN.
5. UNLESS BGC AGREES OTHERWISE IN WRITING, THIS DRAWING SHALL NOT BE MODIFIED OR USED FOR ANY PURPOSE OTHER THAN THE PURPOSE FOR WHICH BGC GENERATED IT. BGC SHALL HAVE NO LIABILITY FOR ANY DAMAGES OR LOSS ARISING IN ANY WAY FROM ANY USE OR MODIFICATION OF THIS DOCUMENT NOT AUTHORIZED BY BGC. ANY USE OF OR RELIANCE UPON THIS DOCUMENT OR ITS CONTENT BY THIRD PARTIES SHALL BE AT SUCH THIRD PARTIES' SOLE RISK.

	1:1,000,000
DATE:	MAY 2022
DRAWN:	RDC
CHECKED:	PQ
APPROVED:	KH

BGC ENGINEERING INC.
AN APPLIED EARTH SCIENCES COMPANY

CLIENT: Geohazards International

Coseismic Landslide Susceptibility Mapping for the Kingdom of Bhutan

TITLE: Results for M8 Earthquake Scenario

PROJECT No.: BGC21006

DWG No: 002

C:\Users\rcarter\BGC Engineering Inc\BGC_Squared - GHI Bhutan - GHI Bhutan\04_Reporting\03_Report\FINAL\m8.mxd